nature medicine

Resource

https://doi.org/10.1038/s41591-023-02602-2

An integrated gene-to-outcome multimodal database for metabolic dysfunction-associated steatotic liver disease

Received: 12 April 2023

Accepted: 20 September 2023

Published online: 30 October 2023

Check for updates

Timothy J. Kendall[1,2,13], Maria Jimenez-Ramos[1,13], Frances Turner[3], Prakash Ramachandran[1], Jessica Minnier[4,5], Michael D. McColgan[6], Masood Alam[6], Harriet Ellis[6], Donald R. Dunbar[3], Gabriele Kohnen[7], Prakash Konanahalli[7], Karin A. Oien[7], Lucia Bandiera[8,9], Filippo Menolascina[8,9], Anna Juncker-Jensen[10], Douglas Alexander[11], Charlie Mayor[11], Indra Neil Guha[12] & Jonathan A. Fallowfield[1] ✉

Metabolic dysfunction-associated steatotic liver disease (MASLD) is the commonest cause of chronic liver disease worldwide and represents an unmet precision medicine challenge. We established a retrospective national cohort of 940 histologically defined patients (55.4% men, 44.6% women; median body mass index 31.3; 32% with type 2 diabetes) covering the complete MASLD severity spectrum, and created a secure, searchable, open resource (SteatoSITE). In 668 cases and 39 controls, we generated hepatic bulk RNA sequencing data and performed differential gene expression and pathway analysis, including exploration of gender-specific differences. A web-based gene browser was also developed. We integrated histopathological assessments, transcriptomic data and 5.67 million days of time-stamped longitudinal electronic health record data to define disease-stage-specific gene expression signatures, pathogenic hepatic cell subpopulations and master regulator networks associated with adverse outcomes in MASLD. We constructed a 15-gene transcriptional risk score to predict future hepatic decompensation events (area under the receiver operating characteristic curve 0.86, 0.81 and 0.83 for 1-, 3- and 5-year risk, respectively). Additionally, thyroid hormone receptor beta regulon activity was identified as a critical suppressor of disease progression. SteatoSITE supports rational biomarker and drug development and facilitates precision medicine approaches for patients with MASLD.

Metabolic dysfunction-associated steatotic liver disease (MASLD), previously termed non-alcoholic fatty liver disease (NAFLD)[1], is a growing and underappreciated global public health concern affecting more than one in four adults (over two billion people) and imposing a substantial burden of ill health and socioeconomic problems[2,3]. It is characterized by the presence of cardiometabolic risk factors such as obesity, type 2 diabetes, hypertension and dyslipidemia and is associated with increased morbidity and mortality from cardiovascular disease, chronic kidney disease and many cancers. The histopathological spectrum of MASLD includes isolated fatty liver (simple steatosis) and metabolic dysfunction-associated steatohepatitis (MASH), previously termed non-alcoholic steatohepatitis (NASH), the inflammatory subphenotype

A full list of affiliations appears at the end of the paper. ✉e-mail: Jonathan.Fallowfield@ed.ac.uk

of MASLD that can lead to progressive liver fibrosis, cirrhosis and hepatocellular carcinoma (HCC). Notably, over the past ten years, there has been a tenfold increase in the number of patients with MASLD-related cirrhosis who require a liver transplant[4], and Bayesian modeling forecasts a staggering global prevalence rate of 55.7% by 2040 (ref. 5).

The pathogenesis of MASLD is complex and multifactorial[6,7]. The primary insult of excess lipid accumulation ('substrate overload') is followed by variable contributions from pathogenic drivers including lipotoxicity and immune-mediated inflammation, and disease progression is further enhanced or suppressed by modifiers such as genetic variants[8] and gut microbiota dysbiosis[9,10]. Crucially, not all people with a fatty liver go on to develop adverse liver-related events or die[11], but there is a critical lack of prognostic biomarkers to enable innovations in clinical care pathways and personalized approaches in MASLD. The importance of histological fibrosis in predicting outcomes in MASLD has been highlighted by several studies[11–13], with discrete fibrosis stages dramatically influencing the risk of all-cause mortality and liver-related morbidity and mortality. Yet fibrosis progression rates and outcome prediction in patients remain uncertain, and clinical trials that have been used post hoc to understand the natural history of MASLD are limited by selection bias and rigid entry criteria[14].

There are no licensed pharmacotherapies for MASLD. Numerous drugs with plausible biological targets have failed to show robust efficacy in late-phase interventional trials, especially in patients with cirrhosis[15]. Consequently, the field is shifting focus to combination drug regimens, and, increasingly, researchers are leveraging patient-centered big data to bolster drug discovery efforts[16]. However, the most efficacious drugs and therapeutic combinations to mitigate adverse clinical outcomes in MASLD remain undefined.

To address these issues and provide a resource suitable for the development of precision medicine strategies in MASLD, we established SteatoSITE: to our knowledge, the world's first data commons[17] for MASLD research. SteatoSITE integrates multimodal multiscale retrospective data at a national level from 940 cases across Scotland, consisting of quantitative histopathological assessment of archival liver tissues, hepatic bulk RNA sequencing (RNA-seq) and routine clinical data extracted from electronic health records (EHRs) and other administrative sources. Distinctively, SteatoSITE is outcome-rich, with data curated in a longitudinal time-stamped format comprising 5.67 million days of clinical follow-up, enabling translational analyses to elucidate the pathogenesis of MASLD and accelerating the discovery of potential prognostic biomarkers and tractable therapeutic targets. Here, we describe and use this unique resource, providing a comprehensive analysis of hepatic gene expression and cell-type composition across the complete MASLD spectrum by identifying transcription-factor-regulated gene networks (regulons) associated with disease progression and developing a novel transcriptome-based risk-prediction model for hepatic decompensation.

Results

Cohort composition

SteatoSITE is a secondary-care, outcome-enriched cohort of 940 cases from the three participating NHS Scotland Biorepositories (Lothian, Greater Glasgow, and Clyde and Grampian) (Fig. 1a), representing the full histological spectrum from normal liver tissue to MASLD-related cirrhosis. Demographic and phenotypic characteristics of the cohort are shown in Table 1. Cases with a liver tissue sample acquired between January 2000 and October 2019 were selected. All patients were ≥18 years of age at the tissue sampling date. Data from EHRs and national datasets were retrieved, where available, from a period between ten years before the tissue sampling date until May 2020, comprising more than 5.67 million days (or roughly 15,547 years) of comprehensive routine clinical data, and annotated patient timelines were created (Fig. 1b and Supplementary Table 1). Further detail of the temporal coverage of blood test results is shown in Supplementary Table 2. Indications for biopsy or resection on the basis of a review of the information submitted with each specimen as part of routine clinical care are shown in Supplementary Table 3. The post-tissue sampling periods for biopsies, resections and explants are shown in Extended Data Fig. 1a.

Histopathological characterization

Scans of hematoxylin and eosin (H&E)- and picrosirius red (PSR)-stained sections from each case were assessed by one of three consultant pathologists with a specialist interest in liver pathology. From the H&E-stained sections, NAFLD activity scores (NASs), components of the Steatosis, Activity and Fibrosis (SAF) scoring system and a score-independent clinical histological diagnosis of NASH were given. From the PSR-stained sections, a NASH-Clinical Research Network (NASH-CRN) and modified Ishak score for staging of fibrosis were given. The inter-rater agreement levels of the scoring pathologists (Supplementary Table 4), assessed on a set of 20 cases after the scoring-harmonization exercise, were at the upper end of the expected ranges[18,19]. Spearman's rho correlation coefficient was used to assess the relationship between modified Ishak fibrosis scores and NASH-CRN fibrosis scores, demonstrating the expected strong positive correlation ($r_s = 0.98$, $P < 2.2 \times 10^{-16}$).

Of the 940 cases, 659 were needle biopsies, 225 were from hepatic resections and 56 were explants for clinically end-stage NAFLD cirrhosis. A clinical histological diagnosis of NASH was given in 455 (48.4%) cases (Extended Data Fig. 1b). Roughly equal numbers of cases were scored at each point of the NASH-CRN fibrosis scale. The relationship of the NAS components and the NASH-CRN fibrosis score are shown in Fig. 1c, and those of the SAF system with modified Ishak fibrosis stage are shown in Extended Data Fig. 1c.

A pixel classifier was trained to identify fat and PSR-positive tissue in scans of PSR-stained sections (Extended Data Fig. 1d). All classified images were manually quality-controlled, and any images containing large fragments of liver capsule, large portal tracts or hilar tissue or with an artifact that was easily ignored during subjective assessment but erroneously computationally classified were removed. The derived fat percentage of the tissue correlated with the assigned steatosis score of the NAS (and SAF) systems, as expected ($r_s = 0.53$, $P < 2.2 \times 10^{-16}$; Extended Data Fig. 1e). The derived PSR-positive percentage of the tissue also correlated with both NASH-CRN ($r_s = 0.61$, $P < 2.2 \times 10^{-16}$; Extended Data Fig. 1f) and modified Ishak ($r_s = 0.61$, $P < 2.2 \times 10^{-16}$; Extended Data Fig. 1g) assigned scores.

Association of histological features with clinical outcomes

The extensive annotation of individual case timelines with clinical data, anchored by the specimen date and retrieved from the EHRs and national datasets, allowed the relationship between data derived from the histological sections and patient outcomes to be examined. Using the 659 needle biopsy cases only, the clear and expected relationship between assigned NASH-CRN fibrosis stage and all-cause mortality was observed (Fig. 1d). Stepwise increases in mortality were evident through progression from stage F0 to F4. An unbiased algorithmic approach to cluster survival curves[20] created two clusters (F0,1,2) and (F3,4),

Fig. 1 | Clinicopathological correlations. a, SteatoSITE Data Commons overview. **b**, Schematic diagram in which horizontal lines are individual patient timelines decorated with a variable amount of multimodal data preceding or following the date of liver tissue sampling (time zero, represented by the vertical yellow line). **c**, Alluvial diagram illustrating the relationship between the scored histopathological features of liver samples. **d**,**e**, Kaplan–Meier time-to-event analysis with log-rank test *P* value for all-cause mortality ($P < 0.0001$) (**d**) and hepatic decompensation events ($P < 0.0001$) (**e**) in patients with biopsies showing early disease (fibrosis stages F0 to F2), bridging fibrosis (stage F3) and cirrhosis (stage F4). A&E, accident and emergency; SFTP, Secure File Transfer Protocol.

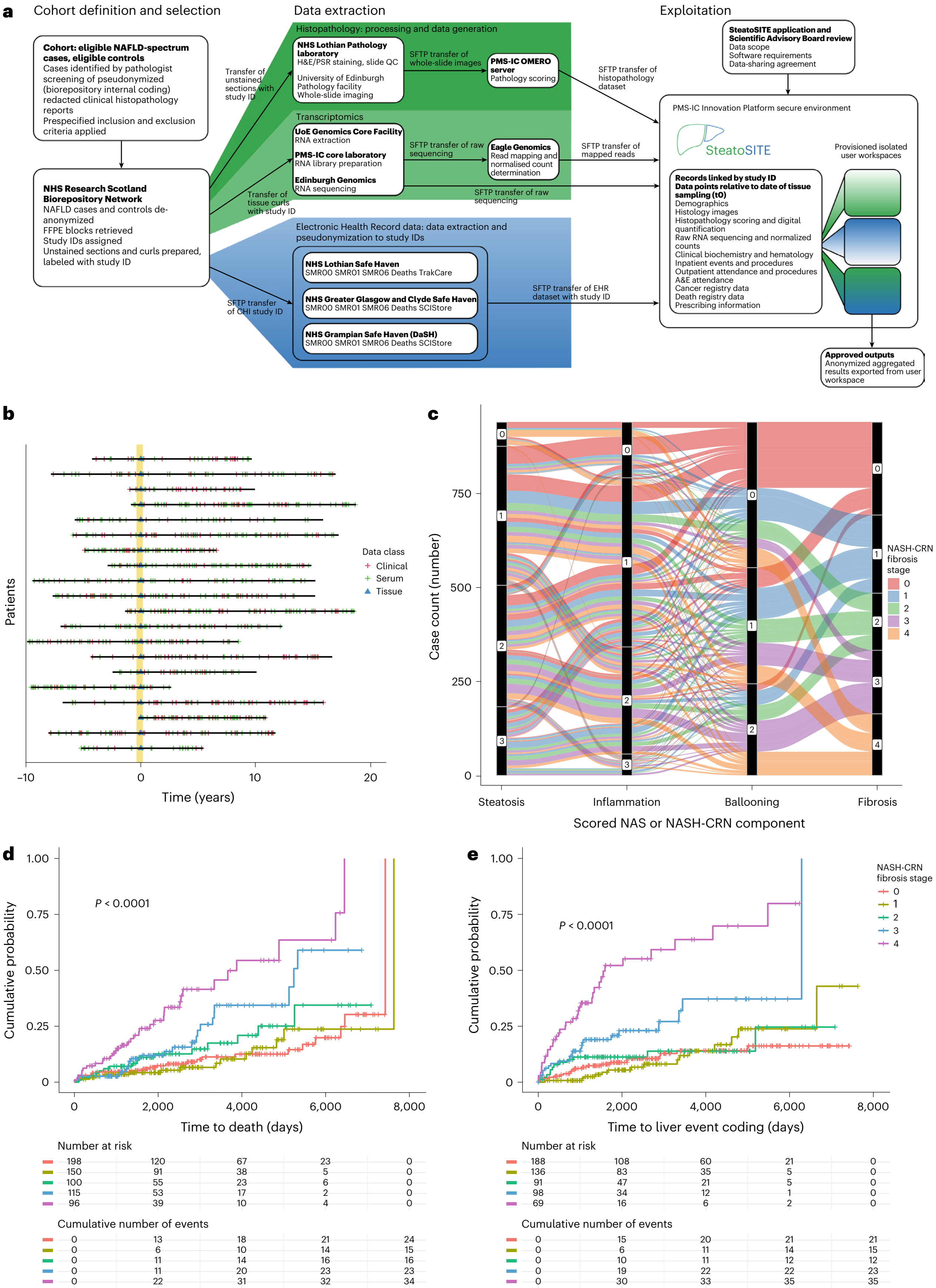
a
Cohort definition and selection
Data extraction
Exploitation
Cohort: eligible NAFLD-spectrum cases, eligible controls
Cases identified by pathologist screening of pseudonymized (biorepository internal coding) redacted clinical histopathology reports
Prespecified inclusion and exclusion criteria applied
NHS Research Scotland Biorepository Network
NAFLD cases and controls de-anonymized
FFPE blocks retrieved
Study IDs assigned
Unstained sections and curls prepared, labeled with study ID
Transfer of unstained sections with study ID
Transfer of tissue curls with study ID
SFTP transfer of CHI study ID
Histopathology: processing and data generation
NHS Lothian Pathology laboratory
H&E/PSR staining, slide QC
University of Edinburgh Pathology facility
Whole-slide imaging
SFTP transfer of whole-slide images
PMS-IC OMERO server
Pathology scoring
SFTP transfer of histopathology dataset
Transcriptomics
UoE Genomics Core Facility
RNA extraction
PMS-IC core laboratory
RNA library preparation
Edinburgh Genomics
RNA sequencing
SFTP transfer of raw sequencing
Eagle Genomics
Read mapping and normalised count determination
SFTP transfer of mapped reads
SFTP transfer of raw sequencing
Electronic Health Record data: data extraction and pseudonymization to study IDs
NHS Lothian Safe Haven
SMR00 SMR01 SMR06 Deaths TrakCare
NHS Greater Glasgow and Clyde Safe Haven
SMR00 SMR01 SMR06 Deaths SCIStore
NHS Grampian Safe Haven (DaSH)
SMR00 SMR01 SMR06 Deaths SCIStore
SFTP transfer of EHR dataset with study ID
SteatoSITE application and Scientific Advisory Board review
Data scope
Software requirements
Data-sharing agreement
PMS-IC Innovation Platform secure environment
SteatoSITE
Provisioned isolated user workspaces
Records linked by study ID
Data points relative to date of tissue sampling (t0)
Demographics
Histology images
Histopathology scoring and digital quantification
Raw RNA sequencing and normalized counts
Clinical biochemistry and hematology
Inpatient events and procedures
Outpatient attendance and procedures
A&E attendance
Cancer registry data
Death registry data
Prescribing information
Approved outputs
Anonymized aggregated results exported from user workspace
b
Patients
Time (years)
−10
0
10
20
Data class
+ Clinical
+ Serum
▲ Tissue
c
Case count (number)
0
250
500
750
Steatosis
Inflammation
Ballooning
Fibrosis
Scored NAS or NASH-CRN component
NASH-CRN fibrosis stage
0
1
2
3
4
d
Cumulative probability
0
0.25
0.50
0.75
1.00
P < 0.0001
Time to death (days)
0
2,000
4,000
6,000
8,000
Number at risk
198 120 67 23 0
150 91 38 5 0
100 55 23 6 0
115 53 17 2 0
96 39 10 4 0
Cumulative number of events
0 13 18 21 24
0 6 10 14 15
0 11 14 16 16
0 11 20 23 23
0 22 31 32 34
e
Cumulative probability
0
0.25
0.50
0.75
1.00
P < 0.0001
Time to liver event coding (days)
0
2,000
4,000
6,000
8,000
NASH-CRN fibrosis stage
0
1
2
3
4
Number at risk
188 108 60 21 0
136 83 35 5 0
91 47 21 5 0
98 34 12 1 0
69 16 6 2 0
Cumulative number of events
0 15 20 21 21
0 6 11 14 15
0 10 11 12 12
0 19 22 22 23
0 30 33 35 35

Table 1 | Demographics and clinical characteristics of SteatoSITE cohort

	NASH-CRN fibrosis stage				
Variable	**0**	**1**	**2**	**3**	**4**
Age, mean (s.d.)					
Years	49.8 (13.9)	53 (14.5)	56.8 (13.6)	59.1 (11.5)	59.9 (9.8)
Gender, number (%)					
Men	137 (55.5)	124 (59.6)	92 (60.5)	85 (50.3)	83 (50.6)
Women	110 (44.5)	84 (40.4)	60 (39.5)	84 (49.7)	81 (49.4)
Ethnicity, number (%)					
White	153 (16.3)	137 (14.6)	90 (9.6)	106 (11.3)	106 (11.3)
Asian	8 (0.9)	6 (0.6)	3 (0.3)	3 (0.3)	2 (0.2)
African	1 (0.1)	0 (0)	0 (0)	0 (0)	0 (0)
Unknown	85 (9)	65 (6.9)	59 (6.3)	60 (6.4)	56 (6)
BMI					
Median (IQR)	30 (7.3)	32.2 (10.3)	31 (5.2)	33.1 (7)	31.7 (7.4)
Unknown BMI, number	175	146	116	120	105
Diabetes, number (%)					
Yes	33 (13.4)	48 (23.1)	42 (27.6)	79 (46.7)	105 (64)
No	214 (86.6)	160 (76.9)	110 (72.4)	90 (53.3)	59 (36)
SIMD quintile, number (%)					
1	21 (2.2)	27 (2.9)	23 (2.4)	29 (3.1)	25 (2.7)
2	19 (2)	30 (3.2)	14 (1.5)	16 (1.7)	26 (2.8)
3	28 (3)	19 (2)	17 (1.8)	21 (2.2)	24 (2.6)
4	23 (2.4)	18 (1.9)	10 (1.1)	14 (1.5)	23 (2.4)
5	43 (4.6)	37 (3.9)	32 (3.4)	36 (3.8)	26 (2.8)
Unknown SIMD	113 (12)	77 (8.2)	56 (6)	53 (5.6)	40 (4.3)
Liver enzymes, median (IQR)					
ALT (U per l)	66 (78)	90 (106.5)	85 (109.5)	77.5 (98.75)	53 (110.25)
AST (U per l)	38 (29)	49 (42)	48 (36.25)	53 (46)	44.5 (37.5)
ALP (U per l)	88 (50.5)	82.5 (43.75)	81 (47)	93.5 (53.5)	107 (69)
Bilirubin (µmol per l)	11 (9)	11 (8.25)	12 (10)	14 (12)	19 (37.5)
Other laboratory results, median (IQR)					
Prothrombin time (s)	12 (2)	12 (2)	12 (2)	13 (1.25)	14 (7)
INR	1 (0.1)	1 (0.1)	1 (0.1)	1.1 (0.2)	1.2 (0.4)
Albumin (g per l)	40 (10)	39 (8)	38 (12)	37 (9)	33.5 (16)
Platelets (×10^9 per l)	237 (100)	230 (94)	213 (96.5)	198 (104.75)	130.5 (103)
Creatinine (µmol per l)	73 (17)	72 (21)	75 (18.25)	70 (22)	71 (26)
Non-invasive tests, median (IQR)					
FIB-4	1 (1)	1.1 (1.2)	1.4 (1.2)	1.8 (1.8)	2.4 (1.9)
Transient elastography (kPa)	8.2 (5.7)	10.9 (5.5)	12.3 (6.9)	14.4 (9.4)	27.3 (34.3)
Prescription, number (%)					
Statin	19 (7.7)	32 (15.4)	18 (11.8)	27 (16)	32 (19.5)
Non-selective beta blocker	1 (0.4)	1 (0.5)	5 (3.3)	4 (2.4)	7 (4.3)
Specimen type, number (%)					
Biopsy	198 (80.2)	150 (72.1)	100 (65.8)	115 (68)	96 (58.5)
Explant	0 (0)	0 (0)	0 (0)	2 (1.2)	54 (32.9)
Resection	49 (19.8)	58 (27.9)	52 (34.2)	52 (30.8)	14 (8.5)
Total case number	247	208	152	169	164

ALP, alkaline phosphatase; ALT, alanine transaminase; AST, aspartate transaminase; FIB-4, fibrosis 4; INR, international normalized ratio; IQR, interquartile range; s.d., standard deviation; U per l, units per liter; µmol per l, mircomoles per liter.

supporting the hypothesis that fibrous bridging of vascular structures is a critical pathophysiological event with prognostic importance in progressive fibrogenesis.

Standard Cox regression modeling of all-cause mortality using age at biopsy, gender and NASH-CRN fibrosis stage as covariates showed that age and NASH-CRN fibrosis stage F4 were independently associated with higher all-cause mortality (Supplementary Table 5). Median intervals to death and censoring of included cases are shown in Supplementary Table 6. A 'pathology scoring only' model was also examined; only fibrosis stage was predictive of survival on multivariate analysis (Supplementary Table 7).

The predictive value of the computationally derived PSR-positive proportion in the biopsy cases where a value was available was also separately examined. Increased PSR content in a biopsy was associated with increased risk of death, hazard ratio 1.06 (95% confidence interval 1.045–1.075, $P < 2 \times 10^{-16}$). To illustrate the potential value of computational pathology in providing prognostic information about overall survival, maximally selected rank statistics were used to determine the optimal PSR percentage cutpoint that divided samples into high- and low-risk groups; the Kaplan–Meier estimator curves are shown in Extended Data Fig. 1h.

The annotated patient timeline of 183 of the 659 biopsy cases contained an outcome coding for at least one of the events defined by expert consensus to represent decompensation in cirrhotic patients[21] or, using UK Operations/Procedure coding data, identifying activity relating to cirrhosis-related hospital admissions[22]. This high number of events contrasts with a published prospective observational study[11]. In SteatoSITE, using only the 106 cases for which an event coding related to decompensation was not present on the patient timeline before the biopsy, F3 and F4 NASH-CRN fibrosis stage was predictive of subsequent decompensation (Fig. 1e). Kaplan–Meier estimator curves for liver-related events (excluding death) associated with F0, F1 and F2 were placed in the same cluster by an unbiased clustering approach, but those associated with F3 and F4 were distinct.

Cox regression modeling of hepatic decompensation events on the cause-specific hazard, with death as a competing risk, using age at biopsy, gender and NASH-CRN fibrosis stage, showed that NASH-CRN fibrosis stages F3 and F4 were associated with increased decompensation events (Supplementary Table 8); Fine–Gray regression for the proportional-hazards modeling of the subdistribution hazard is also reported. Median intervals to decompensation or censoring (death or end of follow-up) of included cases are shown in Supplementary Table 9. A 'pathology scoring only' model for hepatic decompensation (with death as a competing risk) was also examined; only fibrosis stage was predictive of hepatic decompensation on multivariate analysis (Supplementary Table 10).

The value of the computationally derived PSR-positive proportion in the biopsy cases where a value was available was also separately examined for hepatic decompensation, with death as a competing risk. Increased PSR content in a biopsy was associated with increased risk of hepatic decompensation, hazard ratio 1.07 (95% confidence interval 1.05–1.08, $P < 2 \times 10^{-16}$). To illustrate the potential value of computational pathology in providing prognostic information about hepatic decompensation, maximally selected rank statistics were used to determine the optimal PSR percentage cutpoint that divided samples into high- and low-risk groups; the Kaplan–Meier estimator curves are shown in Extended Data Fig. 1i.

Finally, the development of HCC is a low-frequency outcome in MASLD. The complete SteatoSITE cohort includes 80 patients with a coding of HCC at any point in their annotated timeline. The increased risk of HCC in patients with non-cirrhotic MASLD is also well-recognized[23,24]. The SteatoSITE cohort includes 227 resection specimens, with HCC being present in the annotated patient timeline in 44 of these. Notably, 36 of these cases did not have histopathological evidence of cirrhosis in the background liver (Extended Data Fig. 1j). Focusing only on the liver biopsy cases in which no event coding for HCC was present before the biopsy, ten patients received a subsequent coding of HCC in the follow-up period included in the data commons, and assigned NASH-CRN F4 fibrosis stage at biopsy was predictive of the subsequent development of HCC (Extended Data Fig. 1k).

Transcriptomic profiling

The SteatoSITE cohort includes high-quality hepatic RNA-seq data in 668 out of the 940 total cases (comprising 538 biopsies, 39 explants and 130 resections), after applying prespecified quality-control criteria appropriate for archival formalin-fixed paraffin-embedded (FFPE) samples, including the percentage of RNA fragments > 200 nucleotides (DV_{200}) > 30% (ref. 25). Overall, larger liver-resection tissues yielded poorer RNA quality compared with much smaller needle biopsy specimens, likely related to sample fixation.

Normal liver controls ($n = 39$) were also retrieved from the biorepositories for comparative RNA-seq analysis. To confirm the suitability of these control samples, we showed that their transcriptional profile strongly correlated with normal liver samples from independent hepatic RNA-seq datasets[26,27] (average $r_s > 0.9$, adjusted $P < 2 \times 10^{-16}$; Extended Data Fig. 2). After applying quality-control checks, 34 control samples were used for further analyses.

We performed RNA-seq variant calling to detect the most relevant and replicated single-nucleotide polymorphisms (SNPs) identified as risk modifiers of MASLD progression (rs738409, rs72613567, rs58542926 and rs641738 in the genes patatin-like phospholipase domain containing 3 (*PNPLA3*), hydroxysteroid 17-beta dehydrogenase 13 (*HSD17B13*), transmembrane 6 superfamily member 2 (*TM6SF2*) and membrane-bound O-acyltransferase domain containing 7 (*MBOAT7*), respectively). The SNP frequency across histological fibrosis stages is shown in Supplementary Table 11. Sequencing coverage of these genes, and therefore the ability to call variants, was variable. However, the rs738409 C>G p.I148M variant in *PNPLA3* (the strongest genetic risk factor for MASLD and its severity) was successfully called in 612 of 668 MASLD samples with RNA-seq available. The prevalence of GG, GC and

Fig. 2 | Hepatic transcriptomic analysis and summary bioinformatics. a, PCA plot for 616 MASLD samples and 34 normal liver control samples after including batch effects as covariates in the linear model. The first PC is displayed on the *x* axis and the second PC on the *y* axis, with the corresponding percentage of total variance explained by each PC. Dots represent individual samples colored according to NASH-CRN fibrosis stage. **b**, UpSet plot of DEGs showing the unique DEGs belonging to individual sets (fibrosis stages F0/1, F2, F3, F4) and the intersection of DEGs across all fibrosis stages. Set sizes are presented as bars, and their composition is described by the bottom panel. **c**,**d**, Dot plots showing the downregulated (**c**) and upregulated (**d**) Kyoto Encyclopedia of Genes and Genomes pathways (Benjamini and Hochberg false discovery rate $q < 0.05$ and fold-change of ≥1) obtained from one-sided gene-set-enrichment analysis for different fibrosis stages (F0/1, F2, F3, F4). The size of the dot is on the basis of gene count enriched in the pathway, and the color of the dot shows the pathway enrichment significance. **e**, FC of the top 20 differentially expressed genes in each fibrotic stage for both men and women. Exemplar dysregulated genes between men and women are highlighted for illustration. The gray color indicates that the genes were not statistically significantly dysregulated for that specific stage. **f**, Dot plot highlighting the differences between the Reactome pathways ($q < 0.05$ and FC ≥1) obtained by one-sided GSEA in men and women in stage F4 compared with controls. setSIZE indicates the total number of genes present in each specific gene set. P.adjust indicates the Benjamini and Hochberg adjusted *P* values. GeneRatio is k/n, where k is the overlap between the genes of interest and the gene set and n is the number of all unique genes of interest. CAM, cell adhesion molecule; ECM, extracellular matrix; HCM, hypertrophic cardiomyopathy; JAK, Janus kinase; MAPK, mitogen-activated protein kinase; STAT, signal transducer and activator of transcription.

CC genotypes among cases where a call was possible was 16.8%, 27.8% and 54.7%, respectively. After controlling for fibrosis stage, genotype status for predefined variants had no substantial effect on outcomes (data not shown), consistent with findings from a previous long-term follow-up study of 901 individuals with MASLD in which overall mortality was not affected by any genetic variant[28].

For differential gene expression analysis, samples were grouped according to NAS and different fibrosis stages (F0/F1, F2, F3 and F4) and compared with normal liver control samples. The data structure was examined by principal component analysis (PCA). As shown in Fig. 2a, the first two principal components (PCs) explained 8.86% and 7.94% of the observed variation in gene expression. There was modest segregation according to the fibrosis stage.

When samples were classified according to fibrosis stage, we found 218, 478, 1,114 and 2,800 differentially expressed protein-coding genes when comparing F0/F1, F2, F3 and F4 livers with normal liver controls, respectively, and 99 genes differentially expressed in common across stages versus controls (Fig. 2b).

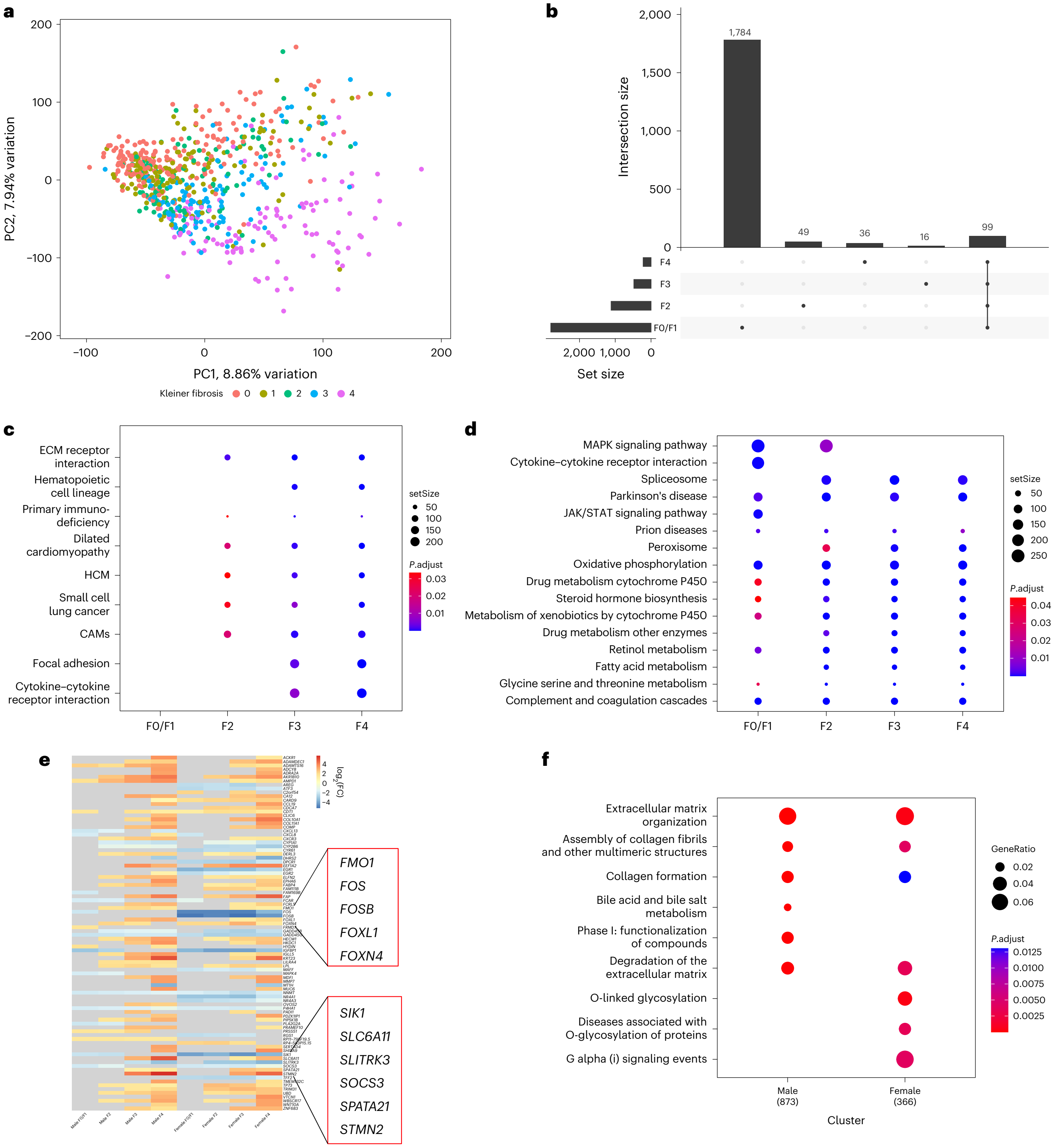

Kyoto Encyclopedia of Genes and Genomes pathways linked to extracellular matrix were enriched from stage F2 onwards, as expected. Notably, other upregulated pathways were those linked to cardiomyopathies ($q < 0.05$; Fig. 2c). In contrast, downregulated genes were enriched for pathways associated with signaling, predominantly in early disease (F0/1), and fatty acid metabolism and peroxisome pathways were enriched from F2 to F4 ($q < 0.05$; Fig. 2d).

When the samples were grouped according to NAS, we identified 203 differentially expressed genes when comparing NAS ≤ 2 ('low NAS') with controls, 621 in the NAS 3–4 group ('borderline NAS') and 793 in the NAS > 4 group ('high NAS'); 182 genes were shared across all NAS groups (Extended Data Fig. 3a). Gene set enrichment analysis (GSEA) revealed, among others, significantly enriched gene ontology terms that participate in 'translation' and the 'immune system' ($q < 0.05$; Extended Data Fig. 3b–d).

As previous studies have highlighted the sexually dimorphic nature of MASLD[29], we also determined gender-specific differences in gene expression and biological pathway enrichment across the MASLD histological spectrum. After stratifying patients by gender and fibrosis stage, we performed differential gene expression analysis to discern shared and gender-specific molecular profiles. In men, we identified 156, 253, 1,167 and 2,767 differentially expressed genes in F0/F1, F2, F3 and F4, respectively, when compared with controls. In women, we identified 383, 768, 1,285 and 2,997 genes in each fibrosis stage, respectively. This indicates that there are more dysregulated genes in women than men. The top 20 differentially expressed genes in each fibrosis stage for both genders are presented in Fig. 2e. Additionally, we performed enrichment analysis between men and women at each stage of fibrosis and observed gender-specific differences in biological pathways. To illustrate, in Fig. 2f, we show that for stage F4, most of the identified pathways are common to both genders, apart from 'bile acid and bile salt metabolism' and 'phase I-functionalization of compounds', which are only present in men. The enriched pathways obtained in other fibrosis stages are shown in Extended Data Fig. 4.

Hence, SteatoSITE enables a comparison of whole-liver gene expression profiles according to histological disease stage. To maximize the accessibility and utility of this resource, we developed an open-access gene browser (https://shiny.igc.ed.ac.uk/SteatoSITE_gene_explorer/), allowing high-level assessment and visualizations of user-selected gene expression according to fibrosis stage.

Cell-type characterization by single-cell deconvolution

Using single-cell RNA-seq (scRNA-seq), we have previously identified distinct populations of scar-associated monocyte-derived macrophages, mesenchymal cells and endothelial cells that populate the fibrotic niche in patients with advanced cirrhosis and interact to regulate liver fibrogenesis[30]. However, the presence of specific pathogenic cellular subpopulations across the full MASLD disease spectrum and how these cells relate to clinical outcomes remain uncertain. To address this, we performed deconvolution of the SteatoSITE bulk RNA-seq data using a publicly available fully annotated scRNA-seq reference dataset compiled from healthy and cirrhotic patients[30] to estimate the proportions of specific hepatic cell types in each SteatoSITE sample and correlate them with histopathological features and patient outcomes.

This analysis demonstrated that the proportion of hepatic scar-associated macrophages (SAMacs), a key regulator of liver fibrosis[30], correlated positively with liver fibrosis stage and steatohepatitis activity across the full MASLD spectrum (Fig. 3a). In contrast, tissue-resident macrophage (Kupffer cell) proportions declined substantially with more advanced fibrosis (Fig. 3a). We validated these transcriptomic findings at the protein level using a bespoke MultiOmyx liver multiplex immunofluorescence (mIF) assay in an independent MASLD histological dataset ($n = 43$), confirming a statistically significant positive correlation of hepatic HLA-DR$^+$CD9$^+$CD14$^+$ SAMac numbers with liver fibrosis stage (Fig. 3b). Positive correlations between mIF SAMac numbers and steatosis, lobular inflammation and ballooning scores were less pronounced than fibrosis stage (Extended Data Fig. 5a–c), mirroring our findings from the deconvolution analysis (Fig. 3a).

Deconvolution analysis also revealed statistically significant positive correlations between fibrosis and the proportion of scar-associated mesenchymal cells, hepatic arterial endothelial cells and lymphatic endothelial cells (Fig. 3a), in keeping with the key roles for mesenchymal cell activation and progressive arterialization of the hepatic microcirculation with loss of normal specialized liver sinusoidal endothelial cell phenotype ('capillarization') in the development of liver fibrosis across the full MASLD spectrum. Interestingly, expansion of plasma cells was also associated with more advanced hepatic fibrosis (Fig. 3a).

Finally, the proportions of cell types, derived by single-cell deconvolution analysis of SteatoSITE bulk RNA-seq data, were examined for their value in predicting adverse clinical outcomes. Strikingly, increased hepatic proportions of SAMacs, scar-associated mesenchymal cells, hepatic arterial endothelial cells, lymphatic endothelial cells and plasma cells were predictive of higher future all-cause mortality (Fig. 3c) and hepatic decompensation events (Fig. 3d). In contrast, higher proportions of more homeostatic liver resident cell types such as vascular smooth muscle cells and liver sinusoidal endothelial cells were protective against future mortality or hepatic decompensation (Fig. 3c,d). Hence, in addition to histology and bulk transcriptomics, changes in the cellular composition of the liver may offer key prognostic information in patients with MASLD.

Transcriptional risk prediction of hepatic decompensation

The annotated patient timelines in SteatoSITE allow predictive tools to be developed. To demonstrate, we used the SteatoSITE RNA-seq data and associated clinical outcomes to develop a novel transcriptome-based risk-prediction model for hepatic decompensation. Such transcriptional risk scores (TRSs) on the basis of transcript abundance are physiologically closer to the phenotype of interest, require smaller training samples and offer greater portability across diverse ancestry groups than polygenic risk scores using genomic variants (SNPs)[31,32].

As the initial feature set, we used the 1,127 protein-encoding genes that were differentially expressed in advanced (F3/F4) compared with early (F0/F1) stage disease ($P < 0.05$, log fold change (FC) ≥1). Univariate Cox regression identified 955 differentially assessed genes (DEGs) as significantly related to decompensation events ($P < 0.01$). To develop a sparse feature set, ten runs of a tenfold lasso-regularized Cox regression were performed, and the coefficients for selected genes were derived (Extended Data Fig. 6a,b). The final TRS predicting hepatic decompensation was composed of the expression of 15 genes: metallothionein 1F (*MT1F*), potassium voltage-gated channel subfamily H member 7 (*KCNH7*), collagen type XXV alpha 1 chain (*COL25A1*), RASD family member 2 (*RASD2*), connective tissue growth factor (*CTGF*),

Fig. 3 | Hepatic bulk RNA-seq data with clinical annotation. a, Corrplots of macrophage, mesenchyme, endothelia and B cell subpopulation proportion correlations with NAS components and NASH-CRN fibrosis stage. $^*P < 0.05$, $^{**}P < 0.01$, $^{***}P < 1 \times 10^{-6}$. Color and size of circles indicate the Pearson correlation coefficients. **b**, Representative H&E-stained sections and multiplex immunofluorescent staining to identify subpopulations of SAMacs, Kupffer cells and tissue monocytes. Selected markers shown. Arrowheads indicate stated cell type. Correlation of number of stated cell type per mm^2 tissue with fibrosis stage ($n = 43$; Spearman's rho and P value indicated). Scale bars, 100 µm. **c**,**d**, Corrplots of macrophage, mesenchyme, endothelia and B cell subpopulation proportion correlations with 1-, 3- and 5-year all-cause mortality (**c**) and decompensation risk (**d**). $^*P < 0.05$, $^{**}P < 0.01$. Color and size of circles indicate the Pearson correlation coefficients.

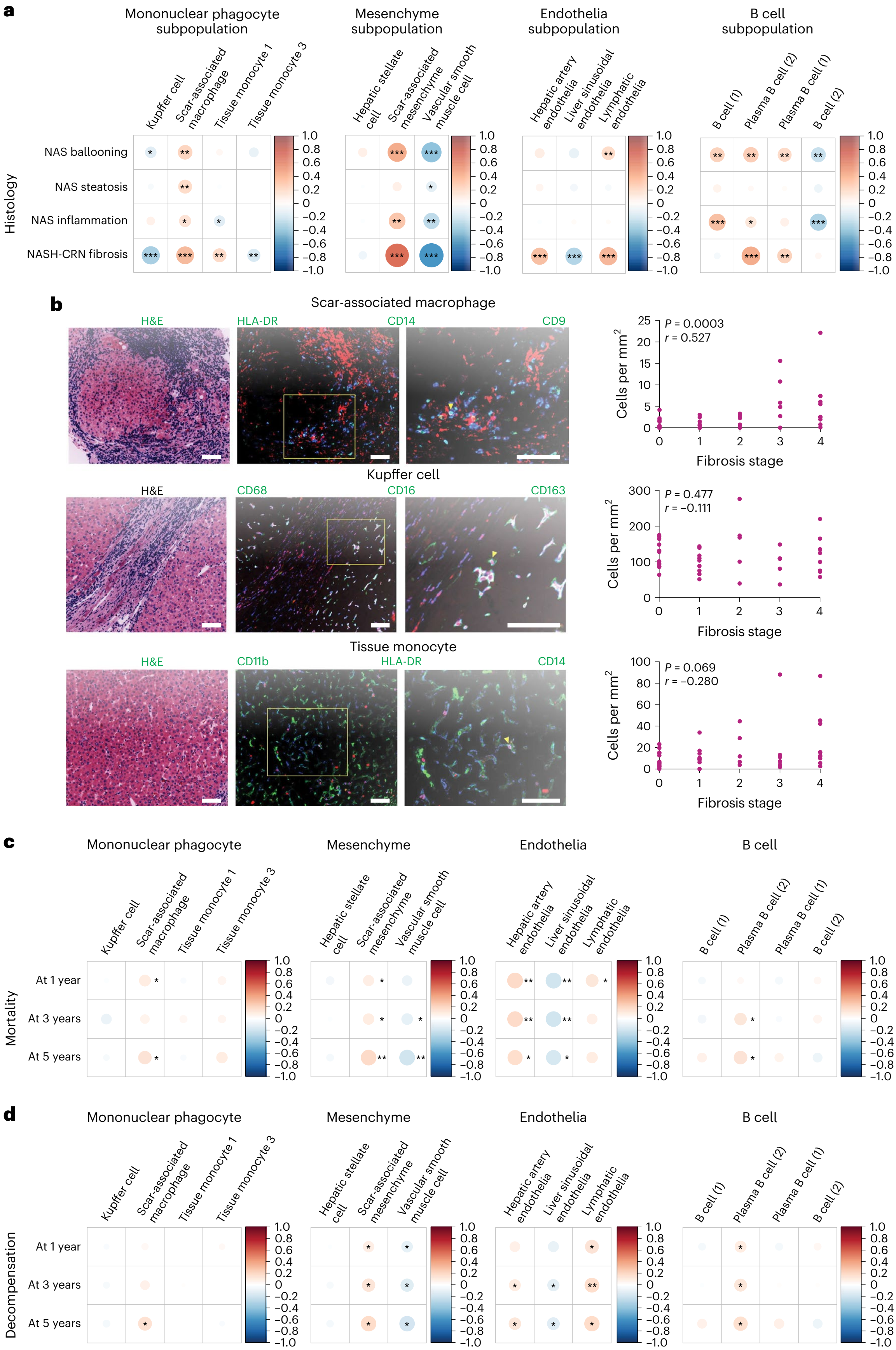
a
Mononuclear phagocyte subpopulation
Mesenchyme subpopulation
Endothelia subpopulation
B cell subpopulation
Kupffer cell
Scar-associated macrophage
Tissue monocyte 1
Tissue monocyte 3
Hepatic stellate cell
Scar-associated mesenchyme
Vascular smooth muscle cell
Hepatic artery endothelia
Liver sinusoidal endothelia
Lymphatic endothelia
B cell (1)
Plasma B cell (2)
Plasma B cell (1)
B cell (2)
Histology
NAS ballooning
NAS steatosis
NAS inflammation
NASH-CRN fibrosis
1.0 0.8 0.6 0.4 0.2 0 −0.2 −0.4 −0.6 −0.8 −1.0
b
Scar-associated macrophage
H&E
HLA-DR
CD14
CD9
Kupffer cell
H&E
CD68
CD16
CD163
Tissue monocyte
H&E
CD11b
HLA-DR
CD14
Cells per mm^2
Fibrosis stage
P = 0.0003
r = 0.527
P = 0.477
r = −0.111
P = 0.069
r = −0.280
0 1 2 3 4
c
Mononuclear phagocyte
Mesenchyme
Endothelia
B cell
Mortality
At 1 year
At 3 years
At 5 years
d
Mononuclear phagocyte
Mesenchyme
Endothelia
B cell
Decompensation
At 1 year
At 3 years
At 5 years

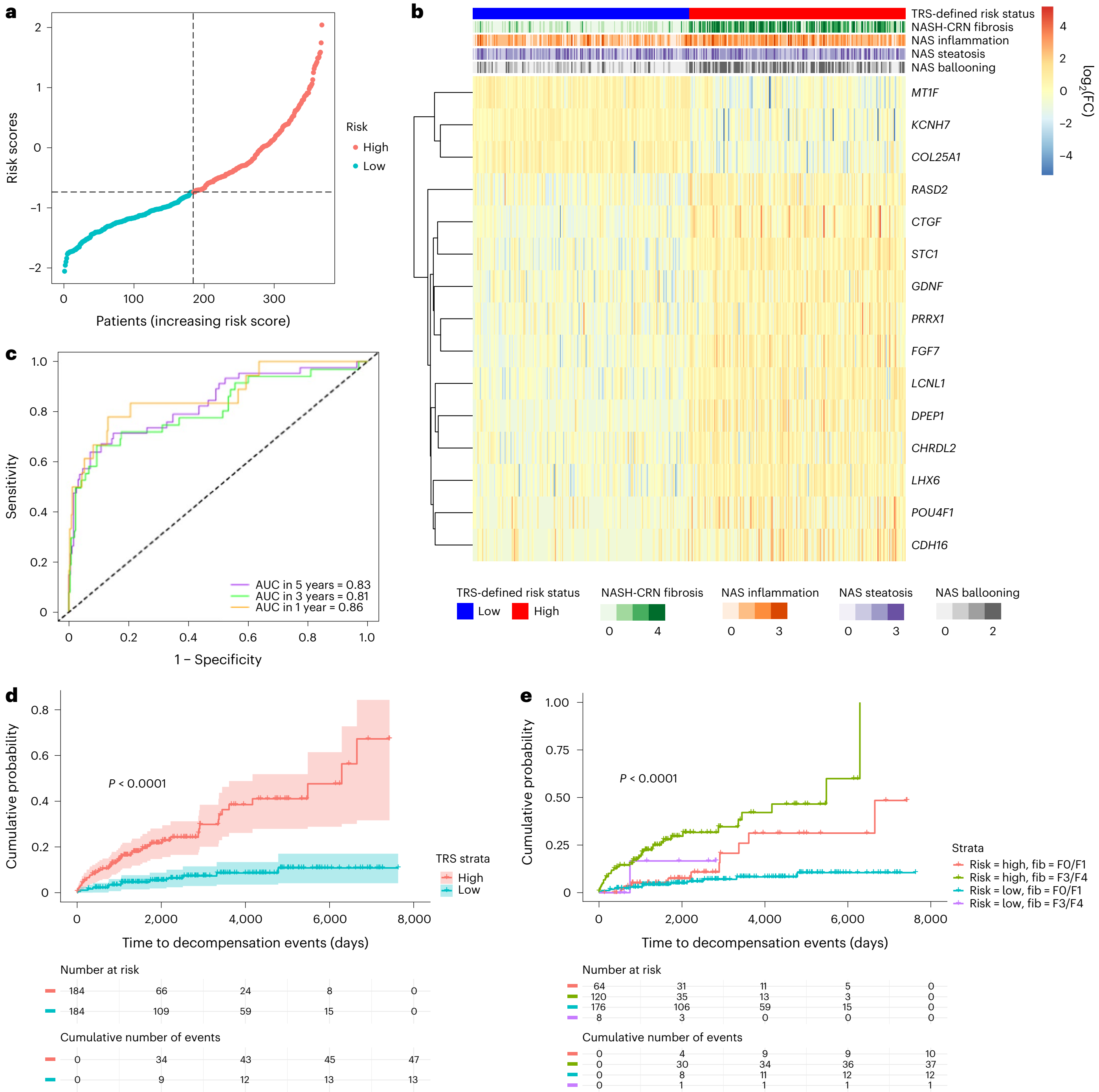

Fig. 4 | Prediction of risk of future decompensation events in advanced fibrosis using hepatic bulk RNA-seq data. a, Correlation between the risk scores and the time of the decompensation events. **b**, Heatmap of the gene expression profile of the prognostic signature. **c**, Time-dependent ROC curves and AUC analyses by the expression of the 15 genes. **d**, Kaplan–Meier curves (with 95% confidence intervals) showing high- and low-risk groups for all biopsy cases; log-rank test *P* value < 0.0001. **e**, Kaplan–Meier curves demonstrating separation of patients into high- and low-risk groups in both mild (F0/1) and severe (F3/4) fibrosis stages; log-rank test *P* value.

stanniocalcin 1 (*STC1*), glial-cell-derived neurotrophic factor (*GDNF*), paired related homeobox 1 (*PRRX1*), fibroblast growth factor 7 (*FGF7*), lipocalin-like 1 (*LCNL1*), dipeptidase 1 (*DPEP1*), chordin-like 2 (*CHRDL2*), LIM homeobox 6 (*LHX6*), POU class 4 homeobox 1 (*POU4F1*) and cadherin 16 (*CDH16*). (Expression across fibrosis stages as plotted by the SteatoSITE gene browser is shown in Extended Data Fig. 7.)

The risk scores were calculated using the formula indicated in the Methods. According to the median risk score, patients were split into high- and low-risk groups (Fig. 4a). Interestingly, samples with a higher risk score had not only a higher fibrosis stage but also a higher hepatocyte ballooning score (Fig. 4b). Time-dependent receiver operating characteristic (ROC) curves were used to assess the predictive ability of the model at specific times after biopsy; the areas under the ROC curves (AUCs) were 86.24% (standard error (SE) 5.11), 80.97% (SE 4.62) and 83.26% (SE 3.86) for 1-, 3- and 5-year risk of decompensation events, respectively (Fig. 4c).

All the biopsy samples could be stratified using the TRS into high- and low-risk groups with substantially different decompensation trajectories. Over postbiopsy follow-up of up to 20 years, those with a high-risk TRS had a cumulative decompensation event probability of more than 0.65 compared with a cumulative probability of 0.11 in those with a low-risk TRS (Fig. 4d). Next, to derive further prognostic information beyond routine fibrosis staging, samples with mild (F0/F1) or advanced (F3/F4) scarring were stratified using the TRS into groups at high or low risk of future decompensation (Fig. 4e). Although there were insufficient F3/F4 patients with a low TRS to enable further categorization of these patients, application of the TRS augmented risk stratification in MASH patients with early-stage fibrosis. Stratification of biopsies with F2 fibrosis is shown in Extended Data Fig. 6c.

Master regulator analysis of disease progression

We sought to further exploit the rich RNA-seq dataset using the high-risk genes identified as prognostically important components of the TRS to derive further biological understanding of the related transcriptional regulatory network (TRN) in MASLD. The TRN, consisting of transcription factors and regulated target genes, was inferred from the whole-gene-expression dataset. Regulons, a set of genes regulated by a specific transcription factor, were constructed for all transcription factors cataloged by ref. 33. A regulon activity score for each sample was estimated using a two-tailed GSEA approach. Regulons cluster on the basis of activity into two broad groups: those with high activity in advanced fibrosis and low activity in early stages and those showing the opposite pattern (Fig. 5a).

To identify which transcriptional networks lie upstream of the expression of high-risk genes representing the TRS, master regulator analysis[34] was undertaken to identify the statistical significance of the overlap between the regulon (gene targets) of each transcription factor and the 15 genes of the TRS, corrected for multiple hypothesis testing. Three regulons (gene networks regulated by AE binding protein 1 (*AEBP1*), thyroid hormone receptor beta (*THRB*) and zinc finger protein basonuclin zinc finger protein 2 (*BNC2*)) contained substantially greater numbers of the TRS genes than expected by chance, indicating that these three networks may be critical to MASLD disease progression leading to decompensation events.

To examine the patterns of activity of these regulons during progression of disease stage, the mean activity scores for each regulon from each NASH-CRN fibrosis stage were used as pseudo-timeseries data for unsupervised soft clustering. AE binding protein 2 (*AEBP2*) regulon activity is in a cluster of regulons whose activity is low in F0–2 but increased in F3 and F4, whereas *BNC2* regulon activity increases more uniformly from F0 to F4. In contrast, *THRB* regulon activity is high in F0 and F1 but decreases as scarring progresses from F2 to F4 (Fig. 5b).

The relationship between the inferred *AEBP1*, *THRB* and *BNC2* regulons is shown in Fig. 5c, annotated with the direction of regulation of each gene target. Most gene targets for *AEBP1* and *BNC2* are positively regulated, whereas *THRB* exerts largely negative regulation of gene targets shared with both *AEBP1* and *BNC2*.

Given the potential suppressive role for *THRB* over disease-promoting core gene targets, and because *THRB* agonists are in current clinical trials for MASLD, we examined *THRB* regulon activity in more detail. In biopsy cases with no hepatic decompensation before biopsy, differential regulon activity was estimated and the predictive value of *THRB* regulon activity for decompensation events examined (Fig. 5d). A ranked *THRB* regulon differential activity plot confirms the negative relationship between *THRB* regulon activity and disease stage in the biopsy-restricted subset, and the Kaplan–Meier plot indicates that lower *THRB* regulon activity is predictive of hepatic decompensation.

However, the predictive value of *THRB* regulon activity may only reflect association with disease stage. To determine whether *THRB* regulon activity was predictive of hepatic decompensation in samples of matched fibrosis stages, maximally selected rank statistics were used to determine the optimal *THRB* regulon activity cutpoint that divided samples into high- and low-risk groups. Using this cutpoint on histologically low-risk samples with F0 and F1 fibrosis, *THRB* regulon activity identified a subset of MASLD patients with high risk of hepatic decompensation (Extended Data Fig. 8). Deriving a new cutpoint in only the histologically advanced stages F3 and F4 allowed stratification into two distinct groups with either rapid or slower progression to a decompensation event (Fig. 5e).

The potential for a personalized approach, for clinical trials or routine practice, using estimated *THRB* regulon activity is illustrated by case studies from the SteatoSITE dataset. Two cases scored F4 (cirrhosis) on PSR-stained sections with high and lower estimated *THRB* activity are shown in Fig. 5f; the patient with estimated *THRB* regulon activity below the derived threshold (top) had a coded decompensation event 224 days after biopsy, but the patient with *THRB* activity above the cutpoint (bottom) did not experience a coded decompensation event in more than 4,500 days of follow-up. At the other end of the disease stage spectrum, two cases that scored F0 on the PSR-stained sections are shown in Extended Data Fig. 8; the case with high estimated *THRB* regulon activity derived from RNA-seq (bottom) was not associated with hepatic decompensation, whereas the case with low estimated *THRB* regulon activity (top) was.

Discussion

We have established what is to the best of our knowledge a unique resource comprising extensive histopathological assessments, transcriptome analysis and rich clinical data across the full MASLD severity spectrum. SteatoSITE is a dataset of broad utility that will enable discovery science, digital pathology research, artificial intelligence approaches and translational studies in MASLD (a subset of the umbrella grouping of steatotic liver disease (SLD)) in the future. Our approach is complementary to continuing global initiatives in MASLD such as biomarker-focused research being conducted by the Liver Investigation: Testing Marker Utility in Steatohepatitis and Non-Invasive BioMarkers of MetaBolic Liver DiseasE[35] consortia, as well as 'omics repositories such as http://liverproteome.org/ and https://www.livercellatlas.org/index.php that contain MASLD and human subsections, respectively. However, crucially, gene signatures and histopathological

Fig. 5 | The relationship of *THRB* with disease progression. a, Heatmap of estimated transcriptional network (regulon) activity across the SteatoSITE dataset. **b**, Patterns of activity and cluster membership of the three regulons (*THRB*, *AEBP2*, *BNC2*). **c**, Relationships of *THRB*, *AEBP1*, *BNC2* regulatory networks with significant numbers of component genes from the TRS as gene target members in disease progression. Red edges, positive regulation of gene target; blue edges, negative regulation of gene target; blue nodes, net negative gene regulation; red nodes, net positive gene regulation; gray nodes, net neutral gene regulation; green nodes, TRS gene member. **d**, Ranked *THRB* regulon differential activity plot confirms the negative relationship between *THRB* regulon activity and disease stage (left and center), and the Kaplan–Meier plot indicates that lower *THRB* regulon activity is predictive of hepatic decompensation (right); log-rank test *P* value. **e**, In histologically identical high-risk fibrosis stages (F3 and F4), low *THRB* activity identifies patients at high risk of hepatic decompensation event; log-rank test *P* value < 0.0001. **f**, Example individual two-tailed gene set enrichment plots of target genes in the *THRB* regulon (left, two-tailed gene set enrichment testing with Benjamini and Hochberg (false discovery rate) adjusted *P* values < 0.001) from two patients with identical F4 stage (cirrhosis) on PSR-stained sections (right), where the patient with low *THRB* differential regulon activity (top, blue) progressed to a hepatic decompensation event 224 days after biopsy in contrast to a patient with high *THRB* regulon activity who did not experience a decompensation event during the 4,500 days until censoring (bottom, red). Scale bars, 2 mm. dES, differential enrichment score.

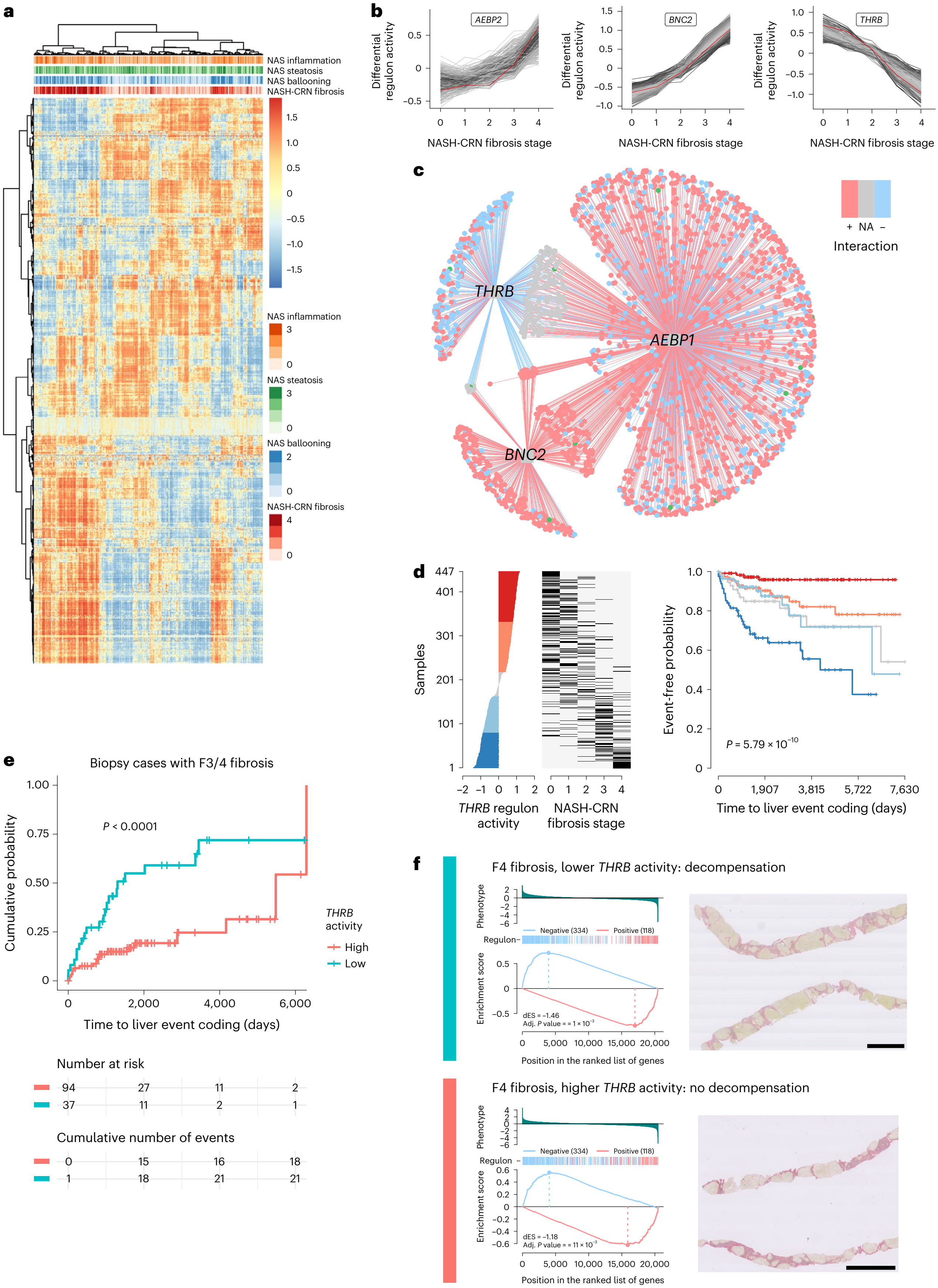
a
NAS inflammation
NAS steatosis
NAS ballooning
NASH-CRN fibrosis
1.5
1.0
0.5
0
−0.5
−1.0
−1.5
NAS inflammation
3
0
NAS steatosis
3
0
NAS ballooning
2
0
NASH-CRN fibrosis
4
0
b
AEBP2
BNC2
THRB
Differential regulon activity
NASH-CRN fibrosis stage
c
THRB
AEBP1
BNC2
+ NA −
Interaction
d
447
401
301
201
101
1
Samples
−2 −1 0 1 2
THRB regulon activity
0 1 2 3 4
NASH-CRN fibrosis stage
Event-free probability
P = 5.79 × 10−10
0 1,907 3,815 5,722 7,630
Time to liver event coding (days)
e
Biopsy cases with F3/4 fibrosis
Cumulative probability
P < 0.0001
0 2,000 4,000 6,000
Time to liver event coding (days)
THRB activity
High
Low
Number at risk
94 27 11 2
37 11 2 1
Cumulative number of events
0 15 16 18
1 18 21 21
f
F4 fibrosis, lower THRB activity: decompensation
Phenotype
Negative (334)
Positive (118)
Regulon
Enrichment score
dES = −1.46
Adj. P value = = 1 × 10−3
0 5,000 10,000 15,000 20,000
Position in the ranked list of genes
F4 fibrosis, higher THRB activity: no decompensation
dES = −1.18
Adj. P value = = 11 × 10−3
Position in the ranked list of genes

metrics in SteatoSITE are linked to clinical outcomes to enable rational diagnostic and treatment approaches for patients with different stages and activity of disease to be determined. Indeed, an authoritative expert review stated that "for more refined treatment of NASH, orthogonal approaches that integrate genetic, clinical and pathological datasets may yield treatments for specific subphenotypes of the disease"[36]. We believe that SteatoSITE provides the relevant multiscale and multimodal data required to meet this challenge.

Consistent with previously published observational data[37], we began by showing the strong positive association between histological fibrosis stage and future clinical outcomes including all-cause mortality, HCC and a composite outcome of hepatic decompensation events. These findings validated the broad content and data integration of the SteatoSITE cohort. We went on to perform a comprehensive bioinformatic analysis of the hepatic bulk RNA-seq data, identifying key genes and enriched gene functions/pathways that characterize discrete histological subtypes and generating disease stage-specific transcriptional profiles to inform drug-target discovery and the development of clinically relevant biomarkers in MASLD. In addition, we provide an open-access web-based gene browser so the scientific community can interactively explore and visualize the SteatoSITE RNA-seq data, thus increasing the accessibility and effect of our work.

As studies have highlighted the sexually dimorphic nature of MASLD[38], we also performed gender-specific analyses to explore differences in gene expression and molecular pathways. Across the MASLD disease spectrum, we identified transcriptional differences and gender-biased enrichment of molecular pathways, such as bile acid and bile salt metabolism and O-linked glycosylation in stage F4 livers. Further work is needed to determine the effect of such differences on disease progression in MASLD, as well as their relevance to biomarkers, therapeutic targets and treatment responses in men and women.

The advent of single-cell transcriptomic technologies is transforming our understanding of the pathobiology of liver diseases including MASLD, identifying key pathogenic cell types and candidate therapeutic targets[39–41]. However, the study of these cell populations across the full disease spectrum remains limited, with minimal data defining which specific cell states are associated with adverse clinical outcomes. Here, we used a single-cell deconvolution approach to interrogate changes in cellular composition in the SteatoSITE cohort, confirming expansion of SAMacs, scar-associated mesenchymal cells, plasma cells, hepatic arterial endothelial cells and lymphatic endothelial cells during MASLD progression. Crucially, expansion of these populations also correlates with poor long-term patient prognosis, highlighting their potential role as therapeutic targets in MASLD and informing novel immunohistochemical approaches to better characterize liver biopsy tissue and identify high-risk patient subphenotypes. Indeed, multiplex immunohistochemistry is already being used to improve stratification in patients with a range of cancers[42–44], so future refinement of our liver macrophage-focused high-plex MultiOmyx assay to include specific markers for pathogenic mesenchymal, endothelial and plasma cells will enable a comprehensive assessment of the liver fibrotic niche from a single slide and may facilitate improved identification of high-risk MASLD patients compared to existing histological approaches.

As the individual patient-level datapoints in SteatoSITE are temporally defined, researchers can perform time-to-event predictions using survival-analysis methods. Here, we illustrated this by showing that hepatic gene expression data in our cohort had a high predictive value for risk of future hepatic decompensation events, over and above standard fibrosis staging. The transition from compensated cirrhosis to decompensated cirrhosis occurs at a rate of about 5% to 7% per year[45]. Decompensation represents a key prognostic inflection point in the natural history of chronic liver disease, as the median survival drops from more than 12 years for compensated cirrhosis to about 2 years for decompensated cirrhosis[45]. However, in patients with advanced fibrosis or cirrhosis (F3/F4), individual risk of decompensation is variable and hard to predict, and preventative therapies are lacking. On the basis of automated variable selection methods to reduce overfitting, we identified a 15-gene panel and derived a risk score that could classify stage-defined MASLD patients into high- or low-risk groups for decompensation[46,47]. To the best of our knowledge, there are no TRSs reported in MASLD; but notably, a TRS approach outperformed static genotypic risk assessment in distinguishing Crohn's disease from healthy samples and predicting complications[48]. Genes represented in our TRS include five members predicted to be secreted proteins, according to The Human Protein Atlas (https://www.proteinatlas.org), which could be explored further in suitably well-annotated clinical samples. Although not previously reported in MASLD, *CHRDL2* is upregulated in a range of tumor tissues including HCC[49], while *STC1*, *CTGF*[50], *GDNF* and *FGF7* are all linked to hepatic fibrogenesis[51,52]. Additionally, *STC1* encodes a secreted glycoprotein reported as a potential serum biomarker for hepatitis B virus-associated liver fibrosis[51], and secreted *FGF7* protein[53] was identified as a prognostic marker in cholangiocarcinoma. The predictive model requires external validation, ideally in prospective longitudinal studies. However, to our knowledge, there are at present no available MASLD datasets with integrated pathology, transcriptomics and clinical outcome data to enable this.

Finally, to search for new and highly effective upstream therapeutic targets, we used high-risk genes from the TRS to uncover core gene networks and master regulators likely to exert influence over disease progression and patient outcomes. Intriguingly, one regulon—*THRB*—was suppressive of the other two identified (*AEBP1* and *BCN2*, which are linked to hepatic fibrogenesis and MASLD progression[54,55]). Moreover, *THRB* regulon activity not only decreased with advancing fibrosis stage but also predicted future hepatic decompensation (beyond standard fibrosis scoring). Liver-targeted thyromimetics selectively activating *THRB*, such as resmetirom (MGL-3196) and VK2809, increase hepatic fat metabolism and reduce lipotoxicity and have recently emerged as leading pharmacological candidates for the treatment of MASLD[56]. Indeed, resmetirom[57] has advanced to phase 3 trials[58], and a MASLD cirrhosis-outcomes trial is underway. Our data reinforce the importance of *THRB* as a therapeutic target with the potential to affect hard clinical endpoints and illustrate how adding transcriptomic information to histology might further stratify prognosis and enable tailoring of treatment.

The creation of SteatoSITE was facilitated by the Scottish demographics and healthcare infrastructure. Multimodal data were drawn from three of the four regional Safe Havens (trusted research environments), covering 12 of the 14 territorial Health Boards, and thus sampling most of the Scottish population. Scotland has a well-established ecosystem for precision medicine consisting of a stable population base of ~5.5 million people, a significant incidence of major chronic disease (death rates from chronic liver disease in Scotland are 70% higher than the UK average[59]), a single healthcare provider (National Health Service (NHS) Scotland) and an EHR system operating on a national scale with a unique common field identifier (Community Health Index (CHI) number) allowing characterization and longitudinal follow-up of well-defined patient cohorts; these key elements differentiate Scotland from many other countries.

Given the scale and complexity of SteatoSITE and its use of routine retrospective multicentric clinical data, several technical and organizational challenges and limitations are acknowledged. Leveraging EHR data for MASLD research is recognized as potentially powerful, but consensus guidelines have only emerged over the past three years[21,60]. Using three different NHS Safe Havens necessitated an exacting and systematic data-cleaning process, including data duplication, human error (for example, incorrect data entry, typographical errors, sample mislabeling), issues with data standardization, errors due to different delimiters/encoding in input files, data formatting and missing data/completeness. Notably, some source data (for example, FibroScan results) are inconsistently recorded across Health Boards and were therefore hard to obtain, even using laborious manual methods. Additionally, there are specific limitations about the cohort itself. Inevitably, using a secondary-care tissue-first selection process introduces inherent spectrum bias. This is a strength in terms of outcome enrichment but means that SteatoSITE will have less value for modeling the population-level natural history of MASLD. Indeed, patient characteristics (higher age and body mass index (BMI)), more frequent comorbidities and baseline disease severity likely explain the higher incidence of outcomes in SteatoSITE compared with other published MASLD cohorts[11,61,62]. The demographic makeup of the SteatoSITE cohort also lacks ethnic diversity (majority white Scottish), so caution is advised about the generalizability of findings to other geographical areas and ethnic populations. Finally, confounding due to unsuspected[63] or poorly recorded alcohol use is a perennial issue in SLD research. To exclude erroneous cases of alcohol-related liver disease in SteatoSITE, we manually reviewed every individual clinical history section of the pathology request forms and each subsequent diagnostic report from the biorepository databases and carefully checked the cause-of-death data. We also collected International Classification of Diseases (ICD)-10 codes for alcohol-use disorders as indicated by consensus guidelines[21]. However, data on alcohol consumption (in grams per week) and drinking patterns are limited by this study's retrospective routine/real-world nature and the lack of detailed and standardized recording of alcohol-related data in historical EHRs. Yet even in prospective studies, alcohol is a likely confounder, as highlighted by the measurement of ethyl glucuronide in hair that detected harmful alcohol consumption in 29% of patients with 'presumed NAFLD'[63]. SteatoSITE has laid the groundwork for a variety of important research themes in MASLD, providing a rich multimodal database to inform drug and biomarker development[64] and a catalog of high-resolution whole-slide images as a valuable testbed for novel digital pathology algorithms. Here we describe SteatoSITE v.1, but our intention is that this resource will be added to and refined, following further research and evolving disease classifications, to enhance its content and operability.

Online content

Any methods, additional references, Nature Portfolio reporting summaries, source data, extended data, supplementary information, acknowledgements, peer review information; details of author contributions and competing interests; and statements of data and code availability are available at https://doi.org/10.1038/s41591-023-02602-2.

References

1. Rinella, M. E. et al. A multi-society Delphi consensus statement on new fatty liver disease nomenclature. *Hepatology* https://doi.org/10.1097/HEP.0000000000000520 (2023).
2. WHO European Region. SDR, chronic liver disease and cirrhosis, all ages, per 100 000. *European Health Information Gateway* https://gateway.euro.who.int/en/indicators/hfa_236-1860-sdr-chronic-liver-disease-and-cirrhosis-all-ages-per-100-000/ (2021).
3. Lazarus, J. V. et al. The global NAFLD policy review and preparedness index: are countries ready to address this silent public health challenge? *J. Hepatol.* **76**, 771–780 (2022).
4. *NHS Blood and Transplant Annual Report and Accounts 2018/19* (NHS Blood and Transplant, 2019).
5. Le, M. H. et al. Forecasted 2040 global prevalence of nonalcoholic fatty liver disease using hierarchical Bayesian approach. *Clin. Mol. Hepatol.* **28**, 841–850 (2022).
6. Loomba, R., Friedman, S. L. & Shulman, G. I. Mechanisms and disease consequences of nonalcoholic fatty liver disease. *Cell* **184**, 2537–2564 (2021).
7. Cai, J., Zhang, X.-J. & Li, H. The role of innate immune cells in nonalcoholic steatohepatitis. *Hepatology* **70**, 1026–1037 (2019).
8. Anstee, Q. M. et al. Genome-wide association study of non-alcoholic fatty liver and steatohepatitis in a histologically characterised cohort. *J. Hepatol.* **73**, 505–515 (2020).
9. Loomba, R. et al. Gut microbiome-based metagenomic signature for non-invasive detection of advanced fibrosis in human nonalcoholic fatty liver disease. *Cell Metab.* **25**, 1054–1062.e5 (2017).
10. Meijnikman, A. S. et al. Microbiome-derived ethanol in nonalcoholic fatty liver disease. *Nat. Med.* **28**, 2100–2106 (2022).
11. Sanyal, A. J. et al. Prospective study of outcomes in adults with nonalcoholic fatty liver disease. *N. Engl. J. Med.* **385**, 1559–1569 (2021).
12. Angulo, P. et al. Liver fibrosis, but no other histologic features, is associated with long-term outcomes of patients with nonalcoholic fatty liver disease. *Gastroenterology* **149**, 389–397.e10 (2015).
13. Vilar-Gomez, E. et al. Fibrosis severity as a determinant of cause-specific mortality in patients with advanced nonalcoholic fatty liver disease: a multi-national cohort study. *Gastroenterology* **155**, 443–457.e17 (2018).
14. Rowe, I. A. & Parker, R. The placebo response in randomized trials in nonalcoholic steatohepatitis simply explained. *Clin. Gastroenterol. Hepatol.* **20**, e564–e572 (2022).
15. Ratziu, V. & Friedman, S. L. Why do so many nonalcoholic steatohepatitis trials fail? *Gastroenterology* https://doi.org/10.1053/j.gastro.2020.05.046 (2020).
16. Chopra, H., Baig, A. A., Gautam, R. K. & Kamal, M. A. Application of artificial intelligence in drug discovery. *Curr. Pharm. Des.* https://doi.org/10.2174/1381612828666220608141049 (2022).
17. Asiimwe, R. et al. From biobank and data silos into a data commons: convergence to support translational medicine. *J. Transl. Med.* **19**, 493 (2021).
18. Kleiner, D. E. et al. Design and validation of a histological scoring system for nonalcoholic fatty liver disease. *Hepatology* **41**, 1313–1321 (2005).
19. Jung, E. S. et al. Interobserver agreement on pathologic features of liver biopsy tissue in patients with nonalcoholic fatty liver disease. *J. Pathol. Transl. Med.* **50**, 190–196 (2016).
20. Villanueva, N. M., Sestelo, M. & Meira-Machado, L. A method for determining groups in multiple survival curves. *Stat. Med.* **38**, 866–877 (2019).
21. Hagström, H. et al. Administrative coding in electronic health care record-based research of NAFLD: an expert panel consensus statement. *Hepatology* **74**, 474–482 (2021).
22. Innes, H. et al. Performance of routine risk scores for predicting cirrhosis-related morbidity in the community. *J. Hepatol.* **77**, 365–376 (2022).
23. Piscaglia, F. et al. Clinical patterns of hepatocellular carcinoma in nonalcoholic fatty liver disease: a multicenter prospective study. *Hepatology* **63**, 827–838 (2016).
24. Stine, J. G. et al. Systematic review with meta-analysis: risk of hepatocellular carcinoma in non-alcoholic steatohepatitis without cirrhosis compared to other liver diseases. *Aliment. Pharmacol. Ther.* **48**, 696–703 (2018).
25. *Evaluating RNA Quality from FFPE Samples* (Illumina, 2015).
26. Govaere, O. et al. Transcriptomic profiling across the nonalcoholic fatty liver disease spectrum reveals gene signatures for steatohepatitis and fibrosis. *Sci. Transl. Med.* **12**, eaba4448 (2020).
27. Suppli, M. P. et al. Hepatic transcriptome signatures in patients with varying degrees of nonalcoholic fatty liver disease compared with healthy normal-weight individuals. *Am. J. Physiol. Gastrointest. Liver Physiol.* **316**, G462–G472 (2019).
28. Holmer, M. et al. Effect of common genetic variants on the risk of cirrhosis in non-alcoholic fatty liver disease during 20 years of follow-up. *Liver Int.* **42**, 2769–2780 (2022).

29. Vandel, J. et al. Hepatic molecular signatures highlight the sexual dimorphism of nonalcoholic steatohepatitis (NASH). *Hepatology* **73**, 920–936 (2021).
30. Ramachandran, P. et al. Resolving the fibrotic niche of human liver cirrhosis at single-cell level. *Nature* **575**, 512–518 (2019).
31. Hu, X. et al. Polygenic transcriptome risk scores for COPD and lung function improve cross-ethnic portability of prediction in the NHLBI TOPMed program. *Am. J. Hum. Genet.* **109**, 857–870 (2022).
32. Liang, Y. et al. Polygenic transcriptome risk scores (PTRS) can improve portability of polygenic risk scores across ancestries. *Genome Biol.* **23**, 23 (2022).
33. Lambert, S. A. et al. The human transcription factors. *Cell* **172**, 650–665 (2018).
34. Carro, M. S. et al. The transcriptional network for mesenchymal transformation of brain tumours. *Nature* **463**, 318–325 (2010).
35. Sanyal, A. J. et al. Diagnostic performance of circulating biomarkers for non-alcoholic steatohepatitis. *Nat. Med.* https://doi.org/10.1038/s41591-023-02539-6 (2023).
36. Friedman, S. L. & Pinzani, M. Hepatic fibrosis 2022: unmet needs and a blueprint for the future. *Hepatology* **75**, 473–488 (2022).
37. Ng, C. H. et al. Mortality outcomes by fibrosis stage in nonalcoholic fatty liver disease: a systematic review and meta-analysis. *Clin. Gastroenterol. Hepatol.* https://doi.org/10.1016/j.cgh.2022.04.014 (2023).
38. Burra, P. et al. Clinical impact of sexual dimorphism in non-alcoholic fatty liver disease (NAFLD) and non-alcoholic steatohepatitis (NASH). *Liver Int.* **41**, 1713–1733 (2021).
39. Ramachandran, P., Matchett, K. P., Dobie, R., Wilson-Kanamori, J. R. & Henderson, N. C. Single-cell technologies in hepatology: new insights into liver biology and disease pathogenesis. *Nat. Rev. Gastroenterol. Hepatol.* **17**, 457–472 (2020).
40. Chu, A. L., Schilling, J. D., King, K. R. & Feldstein, A. E. The power of single-cell analysis for the study of liver pathobiology. *Hepatology* **73**, 437–448 (2021).
41. Wallace, S. J., Tacke, F., Schwabe, R. F. & Henderson, N. C. Understanding the cellular interactome of non-alcoholic fatty liver disease. *JHEP Rep.* **4**, 100524 (2022).
42. Buisseret, L. et al. Clinical significance of CD73 in triple-negative breast cancer: multiplex analysis of a phase III clinical trial. *Ann. Oncol.* **29**, 1056–1062 (2018).
43. Bosisio, F. M. et al. Next-generation pathology using multiplexed immunohistochemistry: mapping tissue architecture at single-cell level. *Front. Oncol.* **12**, 918900 (2022).
44. Ilie, M. et al. Automated chromogenic multiplexed immunohistochemistry assay for diagnosis and predictive biomarker testing in non-small cell lung cancer. *Lung Cancer* **124**, 90–94 (2018).
45. D'Amico, G., Garcia-Tsao, G. & Pagliaro, L. Natural history and prognostic indicators of survival in cirrhosis: a systematic review of 118 studies. *J. Hepatol.* **44**, 217–231 (2006).
46. Bianco, C. et al. Non-invasive stratification of hepatocellular carcinoma risk in non-alcoholic fatty liver using polygenic risk scores. *J. Hepatol.* **74**, 775–782 (2021).
47. De Vincentis, A. et al. A polygenic risk score to refine risk stratification and prediction for severe liver disease by clinical fibrosis scores. *Clin. Gastroenterol. Hepatol.* **20**, 658–673 (2022).
48. Marigorta, U. M. et al. Transcriptional risk scores link GWAS to eQTLs and predict complications in Crohn's disease. *Nat. Genet.* **49**, 1517–1521 (2017).
49. Wu, I. & Moses, M. A. BNF-1, a novel gene encoding a putative extracellular matrix protein, is overexpressed in tumor tissues. *Gene* **311**, 105–110 (2003).
50. Huang, G. & Brigstock, D. R. Regulation of hepatic stellate cells by connective tissue growth factor. *Front. Biosci.* **17**, 2495–2507 (2012).
51. Chan, K. K.-S. et al. Stanniocalcin 1 is a serum biomarker and potential therapeutic target for HBV-associated liver fibrosis. *J. Pathol.* **257**, 227–238 (2022).
52. Tao, L. et al. Glial cell line-derived neurotrophic factor (GDNF) mediates hepatic stellate cell activation via ALK5/Smad signalling. *Gut* **68**, 2214–2227 (2019).
53. Liu, Z. et al. Wnt-TCF7-SOX9 axis promotes cholangiocarcinoma proliferation and pemigatinib resistance in a FGF7-FGFR2 autocrine pathway. *Oncogene* **41**, 2885–2896 (2022).
54. Gerhard, G. S. et al. AEBP1 expression increases with severity of fibrosis in NASH and is regulated by glucose, palmitate, and miR-372-3p. *PLoS ONE* **14**, e0219764 (2019).
55. Bobowski-Gerard, M. et al. Functional genomics uncovers the transcription factor BNC2 as required for myofibroblastic activation in fibrosis. *Nat. Commun.* **13**, 5324 (2022).
56. Wirth, E. K., Puengel, T., Spranger, J. & Tacke, F. Thyroid hormones as a disease modifier and therapeutic target in nonalcoholic steatohepatitis. *Expert Rev. Endocrinol. Metab.* **17**, 425–434 (2022).
57. Harrison, S. A. et al. Effects of resmetirom on noninvasive endpoints in a 36-week phase 2 active treatment extension study in patients with NASH. *Hepatol. Commun.* **5**, 573–588 (2021).
58. Harrison, S. A. et al. Resmetirom for nonalcoholic fattyliver disease: a randomized, double-blind, placebo controlled phase 3 trial. *Nat. Med.* https://doi.org/10.1038/s41591-023-02603-1 (2023).
59. *Chronic Liver Disease: International Comparisons* (The Scottish Public Health Observatory, 2022); https://www.scotpho.org.uk/health-conditions/chronic-liver-disease/data/international-comparisons
60. Shearer, J. E. et al. Systematic review: development of a consensus code set to identify cirrhosis in electronic health records. *Aliment. Pharm. Ther.* **55**, 645–657 (2022).
61. Hagström, H. et al. Fibrosis stage but not NASH predicts mortality and time to development of severe liver disease in biopsy-proven NAFLD. *J. Hepatol.* **67**, 1265–1273 (2017).
62. Boursier, J. et al. Non-invasive tests accurately stratify patients with NAFLD based on their risk of liver-related events. *J. Hepatol.* **76**, 1013–1020 (2022).
63. Staufer, K. et al. Ethyl glucuronide in hair detects a high rate of harmful alcohol consumption in presumed non-alcoholic fatty liver disease. *J. Hepatol.* **77**, 918–930 (2022).
64. Carlessi, R. et al. Single-nucleus RNA sequencing of pre-malignant liver reveals disease-associated hepatocyte state with HCC prognostic potential. *Cell Genom.* **3**, 100301 (2023).

Publisher's note Springer Nature remains neutral with regard to jurisdictional claims in published maps and institutional affiliations.

Open Access This article is licensed under a Creative Commons Attribution 4.0 International License, which permits use, sharing, adaptation, distribution and reproduction in any medium or format, as long as you give appropriate credit to the original author(s) and the source, provide a link to the Creative Commons license, and indicate if changes were made. The images or other third party material in this article are included in the article's Creative Commons license, unless indicated otherwise in a credit line to the material. If material is not included in the article's Creative Commons license and your intended use is not permitted by statutory regulation or exceeds the permitted use, you will need to obtain permission directly from the copyright holder. To view a copy of this license, visit http://creativecommons.org/licenses/by/4.0/.

© The Author(s) 2023

https://doi.org/10.1038/s41591-023-02602-2

[1]Institute for Regeneration and Repair, University of Edinburgh, Edinburgh, UK. [2]Edinburgh Pathology, University of Edinburgh, Edinburgh, UK. [3]Edinburgh Genomics (Bioinformatics), University of Edinburgh, Edinburgh, UK. [4]OHSU-PSU School of Public Health, Oregon Health & Sciences University, Portland, OR, USA. [5]Knight Cancer Institute Biostatistics Shared Resource, Oregon Health & Sciences University, Portland, OR, USA. [6]Precision Medicine Scotland-Innovation Centre (PMS-IC), University of Glasgow, Glasgow, UK. [7]Pathology Department, Queen Elizabeth University Hospital, Glasgow, UK. [8]School of Engineering, Institute of Bioengineering, University of Edinburgh, Edinburgh, UK. [9]Centre for Engineering Biology, University of Edinburgh, Edinburgh, UK. [10]NeoGenomics Laboratories, Fort Myers, FL, USA. [11]NHS Greater Glasgow and Clyde Safe Haven, Glasgow, UK. [12]National Institute of Health Research (NIHR) Nottingham Biomedical Research Centre, Nottingham University Hospitals NHS Trust and University of Nottingham, Nottingham, UK. [13]These authors contributed equally: Timothy J. Kendall, Maria Jimenez-Ramos. ✉e-mail: Jonathan.Fallowfield@ed.ac.uk

https://doi.org/10.1038/s41591-023-02602-2

Methods

Regulatory approvals

Anonymized tissue was supplied after approval by the National Health Service Research Scotland (NRS) Biorepository Network (Reference: SR1032; 2 August 2018). Unified transparent approval for unconsented data inclusion in this pan-Scotland project was provided by the West of Scotland Research Ethics Committee 4 (Reference: 20/WS/0002; 18 February 2020), Public Benefit and Privacy Panel for Health and Social Care (PBPP; Reference: 1819-0091; 4 June 2021), Institutional Research & Development departments and Caldicott Guardians.

Study cohort and sample collection

Initial case selection was on the basis of the availability of archival liver tissue (from biopsies, resections or explants that were surplus to diagnosis) in FFPE blocks available in the NRS Biorepository Network, with the clinical and/or histological diagnosis of NAFLD (MASLD) and meeting the following inclusion/exclusion criteria:

(1) Inclusion criteria—men or women; >18 years of age at the time of tissue sampling; all ethnic groups, socioeconomic backgrounds and health status; dead or alive at the time of inclusion into the data commons.

(2) Exclusion criteria—cases were excluded if any of the following applied: documented history of chronic liver disease of any non-MASLD etiology, including alcohol-related liver disease, chronic viral hepatitis, hemochromatosis, Wilson's disease, autoimmune hepatitis, primary biliary cholangitis, or primary sclerosing cholangitis, and patients with excessive alcohol use documented in the clinical data supplied on the specimen request form (>21 units per week for men, >14 units per week for women) or histological features indicating a secondary non-MASLD diagnosis.

FFPE blocks of normal non-lesional liver from 39 control cases, defined as liver samples without fat deposition or any active primary parenchymal disease, were identified from resection specimens.

Clinical data extraction and processing

After approval from the NHS Scotland PBPP, we obtained relevant unconsented clinical data from three of the four regional Safe Havens that cover 12 of the 14 territorial health boards in Scotland, including demographics (age, gender, ethnicity, Scottish Index of Multiple Deprivation (SIMD)), diagnostic coding (ICD-9, ICD-10) for inpatient and outpatient episodes and procedures (OPCS Classification of Interventions and Procedures (OPCS-4)), routine laboratory blood tests (biochemistry and hematology), liver transient elastography (FibroScan) where available, prescribing information and cancer and death registry data. The comprehensive list of variables (including ICD codes) is shown in Supplementary Table 1. To maximize future comparability and generalizability of results across studies, we followed recent expert consensus guidelines for using administrative coding in EHR-based research of MASLD[21].

The EHR data was uploaded to the Precision Medicine Scotland-Innovation Centre (PMS-IC) Healthcare Landing Zone from the NHS Safe Havens as comma-separated value (.csv) files. In areas where the Safe Havens had poor coverage from their national or regional datasets, further data files were provided by the Biorepository Network. In total, 38 .csv files containing 1,450 columns and 1,055,618 rows were supplied for processing. On upload, data was quality controlled, processed and further minimized to comply with regulatory requirements and ethical approvals.

A Python (v.3.9) script was developed to carry out these data-processing tasks. These included data cleaning, data restructuring and the standardization of file inputs to resolve differences in file encoding, text delimitation and formatting. Where appropriate, differences in data labeling were resolved by adopting the naming conventions used by the NHS Greater Glasgow and Clyde Safe Haven. After standardizing case and spacing, 962 distinct columns remained from the original 1,450 columns. After a more detailed review, columns containing overlapping clinical information were relabeled and merged. This further reduced the dataset to 534 distinct columns, which are present in the final project database.

A final key requirement of the pseudonymization processing was to ensure that all event dates were obfuscated to minimize reidentification risk while allowing for clinically meaningful patient timelines to be established. To achieve this, the duration of time between the specimen acquisition date and the clinical event recorded in the EHR was calculated as Δt in seconds and stored.

Histopathology methods

Blocks for which sufficient tissue was available were assigned a study ID, and samples were cut for histology (3 × 4 μm) and, where possible, RNA extraction (4 × 10 μm). Unstained sections were sent for histological staining by the NHS Lothian pathology laboratory and curls for RNA extraction at the Genetics Core in the Edinburgh Clinical Research Facility. Only NRS biorepository staff independent of the study group held the participant key; they passed data-linkage documents to the local NHS Safe Havens, which were also independent of the study group. No information from the original clinical pathology report was supplied with the sections.

One section from each case was H&E-stained, and one section was PSR-stained. Stained sections of control cases were reviewed to ensure that no histopathological abnormalities were present. Stained sections of MASLD-spectrum cases were scanned at ×20 depth on a Hamamatsu NanoZoomer whole-slide scanner. Whole-slide image files are available as part of the SteatoSITE resource to allow further or repeat subjective or computational analysis by users.

Raw .ndpi files of H&E- and PSR-stained MASLD-spectrum cases were uploaded to a custom server installation of OMERO[65] hosted by PMS-IC (Glasgow, UK).

In June 2019, before SteatoSITE case scoring, three consultant pathologists and participants in the UK National Liver External Quality Assurance scheme (T.J.K., G.K., P.K.) undertook an in-person scoring-harmonization exercise during which examples of histological features scored in the NAS[18] and SAF[66] scoring systems and for staging using NASH-CRN and modified Ishak[67] systems were reviewed. To assess inter-rater performance following this meeting, scans of H&E- and PSR-stained sections from 20 MASLD-spectrum cases including biopsies, explants and resections were each scored by the three pathologists. For ordinal variables, Light's kappa (square weighted, for >2 raters) was calculated using the 'psy'[68] package (v.1.2), and intraclass correlation coefficient, Krippendorf's alpha and Kendall's W were calculated using the 'irr'[69] package (v.0.84.1). For the single scored categorical variable (histological diagnosis of NASH), Light's kappa and Krippendorf's alpha were calculated.

Each pathologist was randomly allocated one-third of the cases and scored the whole-slide images in the OMERO platform, entering the scores as key–value pairs associated with each image (NAS and SAF features for H&E, NASH-CRN and modified Ishak scores for PSR).

A duplexed classification script was applied to the raw .ndpi scans of PSR-stained sections. An initial 'whole tissue' classifier was applied, and small artifacts on the image were removed from the mask on the basis of size. A second pixel classifier of random trees ('RTrees') type with 'gaussian' and 'weighted deviation' features selected, pretrained by one pathologist (T.J.K.), was applied to classify pixels into the histological classes 'fat', 'psr' and 'other tissue' in the 'whole tissue' masked area, and the total number of pixels for each class and the percentage fat and PSR-positive pixels were returned. Whole-slide scan processing was undertaken using command-line execution of a QuPath (v.0.2.3)[70] script on the University of Edinburgh's Edinburgh Compute and Data Facility Linux compute cluster (Eddie). Classified images were reviewed by one pathologist (T.J.K.), independent of all other data, and cases were excluded if large amounts of liver capsule or other artifacts had been included in the classification.

Time-to-event analysis

Analysis using clinical and histopathological data only was undertaken in R[71] (v.4.1.0) using the packages 'survival' (v.3.3-1)[72], 'survminer' (v.0.4.9)[73] and 'finalfit' (v.1.0.5)[74]. Only needle biopsy cases were used for time-to-event analysis. Decompensation events in the clinical data extract were those defined by a combination of ICD codes and UK OPCS-4 codes identifying activity relating to cirrhosis-related hospital admissions activity[21,22]. Decompensation and HCC event analysis was only undertaken on biopsy cases for which the first decompensation or HCC-related coding was present in the clinical data extract after the biopsy date; and analysis was undertaken using death as a competing risk using Cox regression on the cause-specific hazard and Fine–Gray regression for proportional-hazards modeling of the subdistribution hazard as a recommended comprehensive approach[75]. Kaplan–Meier estimator curves of all-cause mortality or event for assigned NASH-CRN fibrosis stages were compared by log-rank testing corrected for multiple comparisons using the Benjamini and Hochberg method in 'survminer'[72]. Clustering of survival/event curves was determined using a k-means bootstrapped method[20]. Hazard ratios and 95% confidence intervals were derived from standard Cox regression models comparing mortality and rates of new-onset decompensation events with NASH-CRN stage, age at biopsy date and gender as covariates. The assumption of proportional hazards for fitted Cox regression models was verified by examining plots of scaled Schoenfeld residuals against time for each covariate.

Multiplex immunofluorescence

mIF staining was performed using the MultiOmyx platform according to ref. 76. This step was performed using a single 4 µm FFPE slide: for each staining round, two cyanine dye-labeled (Cy3, Cy5) antibodies were paired. A custom multiplex panel was created consisting of 17 markers, for a total of nine rounds of antibody staining performed in sequence on the FFPE slides. In the cases of triggering receptor expressed on myeloid cells 2 (TREM2) and CD9 antigen (CD9), which were applied as primary–secondary antibodies, samples were incubated with primary TREM2 and CD9 antibody followed by incubation with a species-specific secondary antibody conjugated to cyanine 5 or 3 (Cy5 or Cy3). The staining signal was then imaged and followed by a dye-inactivation step, enabling repeated rounds of staining. The proprietary deep learning–based workflow NeoLYTX (v.2.0) was subsequently applied to identify individual cells and perform cell classification for each marker, and the phenotype of each cell was determined through coexpression analysis.

Antibodies for MultiOmyx analysis, by staining order, were rabbit anti-TREM2 (polyclonal, ProteinTech, Catalog no. 13483-1-AP, Vendor Lot ID NG) mouse anti-MNDA (253A, Abcam, Catalog no. ab270556, Vendor Lot ID GR3326911), rabbit anti-CD9 (EPR2949, Abcam, Catalog no. ab195422, Vendor Lot ID GR3282696), mouse anti-CD66b (G10F5, BioLegend, Catalog no. 93231, Vendor Lot ID B276347), mouse anti-CD11B (238439, R&D Systems, Catalog no. MAB16992, Vendor Lot ID KGZ0418101), rabbit anti-DC-SIGN (D7F5C, Cell Signaling Technology, Catalog no. 13193, Vendor Lot ID 2), rabbit anti-Ki67 (SP6, Abcam, Catalog no. ab231172, Vendor Lot ID GR3277378), rabbit anti-IDO1 (SP260, Abcam, Catalog no. ab228468, Vendor Lot ID GR3208566), rabbit anti-CD11c (D3V1E, Cell Signaling Technology, Catalog no. 45581BF, Vendor Lot ID 2), rabbit anti-PD-L1 (SP142, Abcam, Catalog no. ab236238, Vendor Lot ID GR3246745), rabbit anti-CD14 (EPR3652, Abcam, Catalog no. ab209971, Vendor Lot ID GR316076), mouse anti-CD16 (DJ130c, Thermo Fisher Scientific, Catalog no. MA1-84008, Vendor Lot ID TK2673378), mouse anti-CD68 (KP1, BioLegend, Catalog no. 98998, Vendor Lot ID B297229), mouse anti-CD163 (EDHu-1, Bio-Rad, Catalog no. MCA1853, Vendor Lot ID 149022A), mouse anti-HLA DQ/DR/DP (WR18, Novus Biologicals, Catalog no. NB100-64358, Vendor Lot ID 1808), mouse anti-CD33 (44M12D3, Novus Biologicals Catalog no. NBP2-22377, Vendor Lot ID 1127455612D3) and mouse anti-SMA (1A4, Sigma-Aldrich, Catalog no. A5228, Vendor Lot ID 037M4805V).

RNA-seq methods

RNA extraction was performed by the Genetics Core (Clinical Research Facility, Western General Hospital, Edinburgh, UK) from 4 × 10 µm curls of FFPE archival human NAFLD liver, using the Qiagen miRNeasy FFPE Kit according to the manufacturer's instructions. Quality control was by Qubit to measure RNA yield (and any potential DNA contamination) and Agilent Bioanalyzer to assess DV_{200}. Samples with DV_{200} below 30% were not progressed for sequencing.

Libraries were prepared at PMS-IC using the low-input Takara Bio SMARTer Stranded Total RNA-Seq Kit v.2 (Pico Input Mammalian).

Sequencing data were generated by Edinburgh Genomics (University of Edinburgh, UK) using the Illumina NovaSeq 6000 platform. Libraries were sequenced over a total of 22 S2 flow cells. Reads were trimmed using 'Cutadapt' (v.cutadapt-1.9.dev2)[77] and aligned to the reference genome (GRCh38) using 'STAR' (v.2.5.2b)[78]. Reads were assigned to features using 'featureCounts3' (v.1.5.1)[79] with a .gtf file from Ensembl (annotation v.84).

For further analyses, R (v.4.1.2) was used. Samples with fewer than one million counts or 70% mapped reads were removed. Any specimen found to include HCC on histological review was excluded from further RNA-seq analyses.

Reads were normalized using the weighted trimmed mean of *M* values method[80]. Differential analysis was carried out with 'limma-voom' (v.3.28.14) with the protein-coding genes. Statistical significance of genes was determined by an adjusted *P* value according to the Benjamini–Hochberg procedure of $P < 0.05$ and absolute FC ≥1 (ref. 81).

PCA was performed to identify covariates that significantly correlated with the main principal components so they could be controlled for downstream analyses (Extended Data Fig. 9). For this reason, gender was included as an additive effect in the linear model used for differential expression when comparing fibrotic stages and NAS score. GSEA[82] was performed with 'clusterProfiler' (v.4.0.5)[83]. Data were visualized with 'ggplot2' (v.3.3.5)[84] and 'clusterProfiler'.

For genes *PNPLA3*, *HSD17B13*, *TM6SF2* and *MBOAT7* containing prespecified variants (rs738409, rs72613567, rs58542926 and rs641738, respectively), the Genome Analysis Toolkit (v.4.0.1.2)[85] was used to call genotypes at all sites. The 'HaplotypeCaller' tool from the Genome Analysis Toolkit was used to produce a single genomic variant call format (GVCF) file per sample, with the following parameters: '--standard-min-confidence-threshold-for-calling 20'; '-dont-use-soft-clipped-bases'; '-L genes.bed'; '-ERC GVCF', where 'genes.bed' is a bed file containing the genome coordinates of the genes of interest (padded by 1 KB in both directions to cover upstream and downstream SNPs). The 'GenotypeGVCFs' tool was then run with the parameter '--include-non-variant-sites' to produce a single VCF file per sample. 'SnpEff' was used to functionally annotate the variants in the VCF files.

The Multi-subject Single-cell Deconvolution tool (v.0.1.1)[86] was run using R (v.3.6.3) to compare the counts from each bulk RNA-seq sample to reference scRNA-seq data from five healthy and five cirrhotic livers[30] to estimate the proportions of each subtype of various lineages of non-parenchymal cells. This was done separately for each of the macrophage (non-circulating), B cells, mesenchyme, endothelial and T-cell lineages. In each analysis, only the scRNA-seq data from cells annotated as belonging to the lineage were used as a reference in the deconvolution, so the sum of estimated proportions of subtypes in each lineage equals one.

To assess the association between histological scores and proportions of various cell subtypes, the Spearman's partial rank correlation coefficient was calculated using the R package 'ppcor' (v.1.1) between the proportion of each subtype and the histological score, accounting for age and gender. Gender was converted to a numerical value by setting 'male' to '1' and 'female' to '2'. The histological data contained the 'fibrosis stage', which includes scores '1a', '1b' and '1c', with '1a' being the least severe and '1c' being the most severe. To perform a rank correlation, these scores were converted to 1, 1.25 and 1.5, respectively. The association between proportion of each subtype and patient outcome (all-cause mortality or a decompensation event) was also assessed using Pearson's correlation. For any given timepoint, samples were given a '0' if the event had not occurred or a '2' if the event had occurred and were excluded if the patient was censored at that time.

Samples with fewer than one million reads assigned to genes in the bulk RNA-seq analysis, that lacked a patient age or that did not come from a biopsy were omitted.

DEGs between F3/F4 and F0/F1 biopsy cases were identified with 'limma-voom' in R. The criteria for statistical significance were adjusted $P < 0.05$ and absolute FC ≥ 1. Univariate Cox analysis was carried out to determine the DEGs associated with decompensation events according to an adjusted $P < 0.01$. Next, lasso-penalized Cox regression was used to filter features using 'glmnet' $\sum_{i=1}^{n} \text{expression}_i \times \text{coefficient}_i$. Patients were divided into high- and low-risk groups according to the median score. Kaplan–Meier analysis was performed using 'survival' (v.3.4-0) and 'survminer' (v.0.4.9) packages. A time-dependent ROC curve was created with the 'timeROC' package (v.0.4) to evaluate the predictive ability of the signature.

Transcriptional network inference and regulon analysis was undertaken in R (v.4.1.0) using the 'RTN' package (v.2.16.0)[87]. Normalized gene expression of all sequenced SteatoSITE samples was used to infer regulons corresponding to all TFs compiled by ref. 33 by permutation analysis with the non-parametric estimator of mutual information and a P value cut-off of 1.75×10^{-7} to correct for multiple hypothesis testing. Unstable gene–TF interactions were removed by bootstrap analysis to produce a consensus network. The ARACNe algorithm[88] using the data-processing inequality theorem to enrich regulons with direct TF–gene target interactions was used to remove the weakest interaction in any triplet composed of two TFs with a common gene target; the threshold for filtering was determined from the null distribution derived in the permutation and bootstrapping steps.

To determine regulon activity scores for each sample, the tni.gsea2() function was used to calculate differential expression of each gene relative to the expression in the entire cohort, and the ranked list of genes was used to form a differential expression signature that was used alongside the TRN to determine differential sample-specific regulon activity.

Regulon activity profiles across disease stage were placed into four clusters by unsupervised soft clustering using the 'Mfuzz' package (v.2.52.0). The fuzzifier parameter, 'm', was directly estimated from the data using mestimate() to apply the method of ref. 89.

The 'RTNsurvival' package (v.1.16.0)[90] was used to undertake time-to-event analysis with *THRB* regulon activity. The cutpoint for *THRB* regulon activity was calculated using surv_cutpoint() from the 'survminer' package, applying maximally selected rank statistics of the 'maxstat' package (v.0.7-25) with a minimum proportion of 0.25.

We developed an open-access gene browser on the basis of the START app[91], which will ultimately be hosted on the SteatoSITE website (https://steatosite.com/). The 'shiny' R package allows the production of interactive plots and charts and is already widely used to allow users to explore RNA-seq data and create their own customized figures. A 'shiny' interface was created to allow scientists to visualize the results of the analysis of differential gene expression according to NASH-CRN fibrosis stage.

Inclusion and ethics statement

SteatoSITE was a consortium project involving the University of Edinburgh, University of Glasgow, NHS Greater Glasgow and Clyde and Eagle Genomics; roles and responsibilities were agreed on among collaborators ahead of the research. The study has included local researchers throughout the research process: study design, study implementation, data ownership, intellectual property and authorship.

Reporting summary

Further information on the research design is available in the Nature Portfolio Reporting Summary linked to this article.

Data availability

Hepatic bulk RNA-seq data are deposited in the European Nucleotide Archive (https://www.ebi.ac.uk/ena; study accession number: PRJEB58625). Gene expression data are also freely available for user-friendly interactive browsing online at https://shiny.igc.ed.ac.uk/SteatoSITE_gene_explorer/. SteatoSITE has delegated ethics from West of Scotland Research Ethics Committee 4 (Reference: 20/WS/0002; 18 February 2020) allowing the granting of access to the full dataset (histopathology scoring, hepatic bulk RNA-seq data, EHR data) only in the PMS-IC secure environment to third parties by application (full details at https://steatosite.com/researchers/), overseen and reviewed by the SteatoSITE Scientific Advisory Board.

Code availability

The codes used for the data analyses in this study can be made available by contacting the corresponding author. Access to codes will be granted for requests for academic use within four weeks of application. R is required software to use the code.

References

65. Allan, C. et al. OMERO: flexible, model-driven data management for experimental biology. *Nat. Methods* **9**, 245–253 (2012).
66. Bedossa, P. et al. Histopathological algorithm and scoring system for evaluation of liver lesions in morbidly obese patients. *Hepatology* **56**, 1751–1759 (2012).
67. McDonald, N. et al. Multiparametric magnetic resonance imaging for quantitation of liver disease: a two-centre cross-sectional observational study. *Sci. Rep.* **8**, 9189 (2018).
68. Falissard, B. psy: various procedures used in psychometrics. R package version 1.2 (2022).
69. Gamer, M., Lemon, J., Fellows, I. & Singh, P. irr: various coefficients of interrater reliability and agreement. R package version 0.84.1 (2019).
70. Bankhead, P. et al. QuPath: open source software for digital pathology image analysis. *Sci. Rep.* **7**, 16878 (2017).
71. R Core Team. *R: A Language and Environment for Statistical Computing* (R Foundation for Statistical Computing, 2022).
72. Kassambara, A., Kosinski, M. & Biecek, P. survminer: drawing survival curves using 'ggplot2'. R package version 0.4.9 (2021).
73. Therneau, T. M. survival: a package for survival analysis in R. R package version 3.5-7 https://CRAN.R-project.org/package=survival (2023).
74. Harrison, E., Drake, T. & Ots, R. finalfit: quickly create elegant regression results tables and plots when modelling. R package version 1.0.6 (2022).
75. Latouche, A., Allignol, A., Beyersmann, J., Labopin, M. & Fine, J. P. A competing risks analysis should report results on all cause-specific hazards and cumulative incidence functions. *J. Clin. Epidemiol.* **66**, 648–653 (2013).
76. Gerdes, M. J. et al. Highly multiplexed single-cell analysis of formalin-fixed, paraffin-embedded cancer tissue. *Proc. Natl Acad. Sci. USA* **110**, 11982–11987 (2013).
77. Martin, M. Cutadapt removes adapter sequences from high-throughput sequencing reads. *EMBnet. J.* **17**, 10–12 (2011).
78. Dobin, A. et al. STAR: ultrafast universal RNA-seq aligner. *Bioinformatics* **29**, 15–21 (2013).

79. Liao, Y., Smyth, G. K. & Shi, W. featureCounts: an efficient general purpose program for assigning sequence reads to genomic features. *Bioinformatics* **30**, 923–930 (2014).
80. Robinson, M. D. & Oshlack, A. A scaling normalization method for differential expression analysis of RNA-seq data. *Genome Biol.* **11**, R25 (2010).
81. Storey, J. D. & Tibshirani, R. Statistical significance for genome-wide studies. *Proc. Natl Acad. Sci. USA* **100**, 9440–9445 (2003).
82. Subramanian, A. et al. Gene set enrichment analysis: a knowledge-based approach for interpreting genome-wide expression profiles. *Proc. Natl Acad. Sci. USA* **102**, 15545–15550 (2005).
83. Wu, T. et al. clusterProfiler 4.0: a universal enrichment tool for interpreting omics data. *Innovation* **2**, 100141 (2021).
84. Wickham, H. *ggplot2: Elegant Graphics for Data Analysis* (Springer, 2016).
85. Van der Auwera, G. A. et al. From FastQ data to high confidence variant calls: the Genome Analysis Toolkit best practices pipeline. *Curr. Protoc. Bioinformatics* **43**, 11.10.1–11.10.33 (2013).
86. Wang, X., Park, J., Susztak, K., Zhang, N. R. & Li, M. Bulk tissue cell type deconvolution with multi-subject single-cell expression reference. *Nat. Commun.* **10**, 380 (2019).
87. Castro, M. A. A. et al. Regulators of genetic risk of breast cancer identified by integrative network analysis. *Nat. Genet.* **48**, 12–21 (2016).
88. Margolin, A. A. et al. Reverse engineering cellular networks. *Nat. Protoc.* **1**, 662–671 (2006).
89. Schwämmle, V. & Jensen, O. N. A simple and fast method to determine the parameters for fuzzy c–means cluster analysis. *Bioinformatics* **26**, 2841–2848 (2010).
90. Groeneveld, C. S. et al. RTNsurvival: an R/Bioconductor package for regulatory network survival analysis. *Bioinformatics* **35**, 4488–4489 (2019).
91. Nelson, J. W., Sklenar, J., Barnes, A. P. & Minnier, J. The START app: a web-based RNAseq analysis and visualization resource. *Bioinformatics* **33**, 447–449 (2017).

Acknowledgements

We are grateful to the following for assistance: L. McMahon, M. McNeil (PMS-IC)—project management, data compliance and security, workspace provision; B. Hartzoulakis (Eagle Genomics) and D. Harbison (PMS-IC)—acquisition of funding; Y. Staeva (Eagle Genomics)—project management; M. Jones (PMS-IC)—RNA-seq libraries; E. Coulston (PMS-IC)—administrative support; Edinburgh Clinical Research Facility Genetics Core/L. Murphy—RNA extraction; Edinburgh Genomics/M. Arno—RNA-seq; electronic Data Research and Innovation Service (eDRIS)/B. Bruce—clinical data access approval; Safe Havens: Lothian (C. Duncan, P. Linksted), Grampian (K. Wilde, J. Lumsden), GG&C (J. Burnie, S. McKenna)—EHR data retrieval; Lothian Bioresource (L. McLeod, C. Marshall)—human liver tissue access; E. McDowall (Institute of Genetics and Cancer)—'shiny' app hosting; SteatoSITE group (Chairperson L. Laidlaw: visiting fellow, University of Bournemouth). This work was funded by Innovate UK ((Precision medicine: impacting through innovative technology (Reference: TS/R017581/1; J.A.F. and T.J.K.)), Innovate UK Eureka (Reference: 105976; J.A.F. and T.J.K.), Guts UK Development Grant (Reference: DGO2019_16; J.A.F., T.J.K., P.R. and F.T.), industrial Collaborative Awards in Science and Engineering (iCASE) PhD studentship funded by the Medical Research Council Precision Medicine Doctoral Training Programme (Reference: MR/R01566X/1; M.J.-R.) and Galecto Biotech (M.J.-R.), Engineering and Physical Sciences Research Council (EPSRC) Innovation Fellowship (Reference: EP/S001921/1; F.M.), EPSRC New Investigator Award (Reference: EP/R035350/1; F.M.), UK Research and Innovation Engineering Biology Transition Award (Reference: BB/W014610/1; F.M.), Wellcome Trust-University of Edinburgh Institutional Strategic Support Fund (Reference: 204804/Z/16/Z; L.B.), EPSRC Postdoctoral Fellowship (Reference: EP/P017134/1; L.B.) and MRC Senior Clinical Fellowship (Reference: MR/W015919/1; P.R.).

Author contributions

J.A.F., T.J.K. and M.D.M. contributed to the development of the study concept and design, and J.A.F., T.J.K., M.J.-R., F.T., H.E., G.K., P.K., P.R., M.D.M., D.R.D., L.B., F.M., A.J.-J., J.M. and I.N.G. contributed to data analysis and interpretation. J.A.F. and T.J.K. drafted the initial manuscript. T.J.K., G.K., P.K., K.A.O., C.M., D.A., D.R.D., M.A. and M.D.M. provided technical and/or material support for the project. J.A.F. is the guarantor of the work. Each author contributed important intellectual content during manuscript drafting or revision and accepts accountability for the overall work by ensuring that questions pertaining to the accuracy or integrity of any portion of the work are appropriately investigated and resolved. All authors approved the final version of the manuscript. The corresponding author attests that all the listed authors meet the authorship criteria and that no others meeting the criteria have been omitted.

Competing interests

T.J.K. serves as a consultant for or has received speakers' fees from Resolution Therapeutics, Clinnovate Health, Perspectum and Incyte Corporation. P.R. serves as a consultant for Merck and has received research grant funding from Genentech. J.A.F. serves as a consultant or advisory board member for Resolution Therapeutics, Kynos Therapeutics, Ipsen, Redx Pharma, River 2 Renal Corp., Stimuliver, Galecto Biotech, Global Clinical Trial Partners and Guidepoint and has received research grant funding from Intercept Pharmaceuticals and Genentech. A.J.-J. is an employee and stock owner at NeoGenomics. I.N.G. serves as an advisory board member for Resolution Therapeutics and has received research grant funding from Gilead Sciences. M.D.M. and D.R.D. have a controlling shareholder interest in Biodev Ltd. The remaining authors declare no competing interests.

Additional information

Extended data is available for this paper at https://doi.org/10.1038/s41591-023-02602-2.

Supplementary information The online version contains supplementary material available at https://doi.org/10.1038/s41591-023-02602-2.

Correspondence and requests for materials should be addressed to Jonathan A. Fallowfield.

Peer review information *Nature Medicine* thanks Maja Thiele, Silvia Sookoian and the other, anonymous, reviewer(s) for their contribution to the peer review of this work. Primary Handling Editor: Jennifer Sargent, in collaboration with the *Nature Medicine* team.

Reprints and permissions information is available at www.nature.com/reprints.

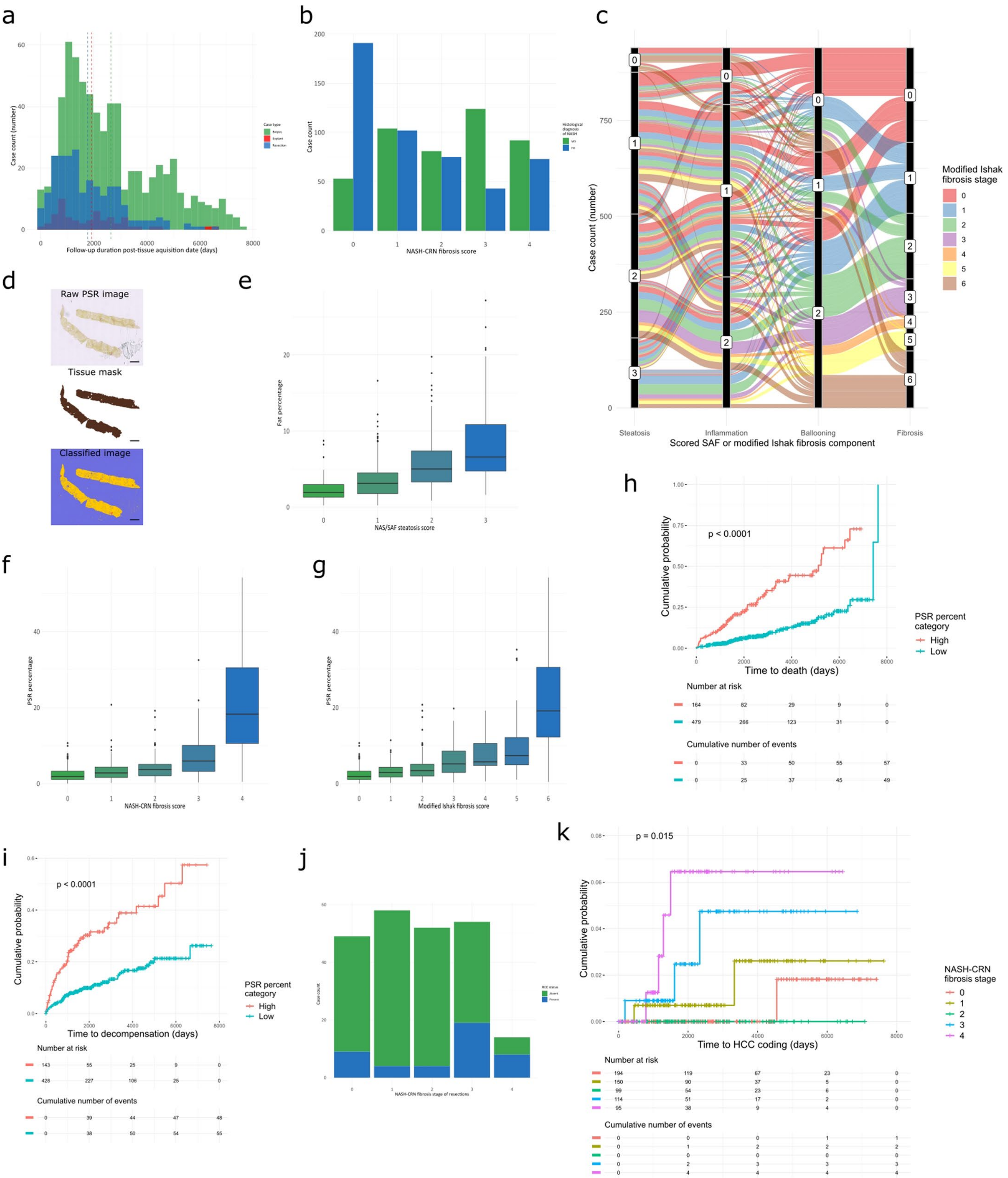

Extended Data Fig. 1 | See next page for caption.

Extended Data Fig. 1 | Additional histopathological analyses. a, Clinical follow-up depth (in days) according to specimen type. **b**, Clinical assessment of the presence or absence of a histological diagnosis of steatohepatitis versus NASH-CRN stage. **c**, Alluvial diagram illustrating the relationship between the scored SAF and modified Ishak stage features. **d**, A representative whole-slide image of a PSR-stained section with the associated tissue mask and applied classifier showing PSR-positive (red) and fat droplets (purple) from the QuPath quantitative pathology pipeline; only pixels present within the tissue mask are used for PSR and fat quantitation. Pixel classification using the same classifier always returns the same values so was only undertaken once. Scale bar, 2 mm. **e**, The amount of steatosis from image quantification versus NAS steatosis assigned scores from the 922 cases with quantifiable whole-slide images. **f**, The PSR percentage from image quantification versus assigned NASH-CRN scores from the 922 cases with quantifiable whole-slide images. **g**, The PSR percentage from image quantification versus assigned modified Ishak scores from the 922 cases with quantifiable whole-slide images. All boxplots show median (centre line), first and third quartiles (lower and upper box limits), 1.5× interquartile range (whiskers). Computationally-derived scar proportion can be used to stratify the risk of all-cause mortality (**h**) and hepatic decompensation (**i**); log–rank test *P*-values < 0.0001. **j**, Count of presence or absence of hepatocellular carcinoma (HCC) in resection cases versus assigned NASH-CRN stage. **k**, Kaplan–Meier time-to-event analysis for HCC in patients with biopsies showing early disease (fibrosis stages F0 to F2), bridging fibrosis (stage F3) and cirrhosis (stage F4); log–rank test *P*-value = 0.015.

https://doi.org/10.1038/s41591-023-02602-2

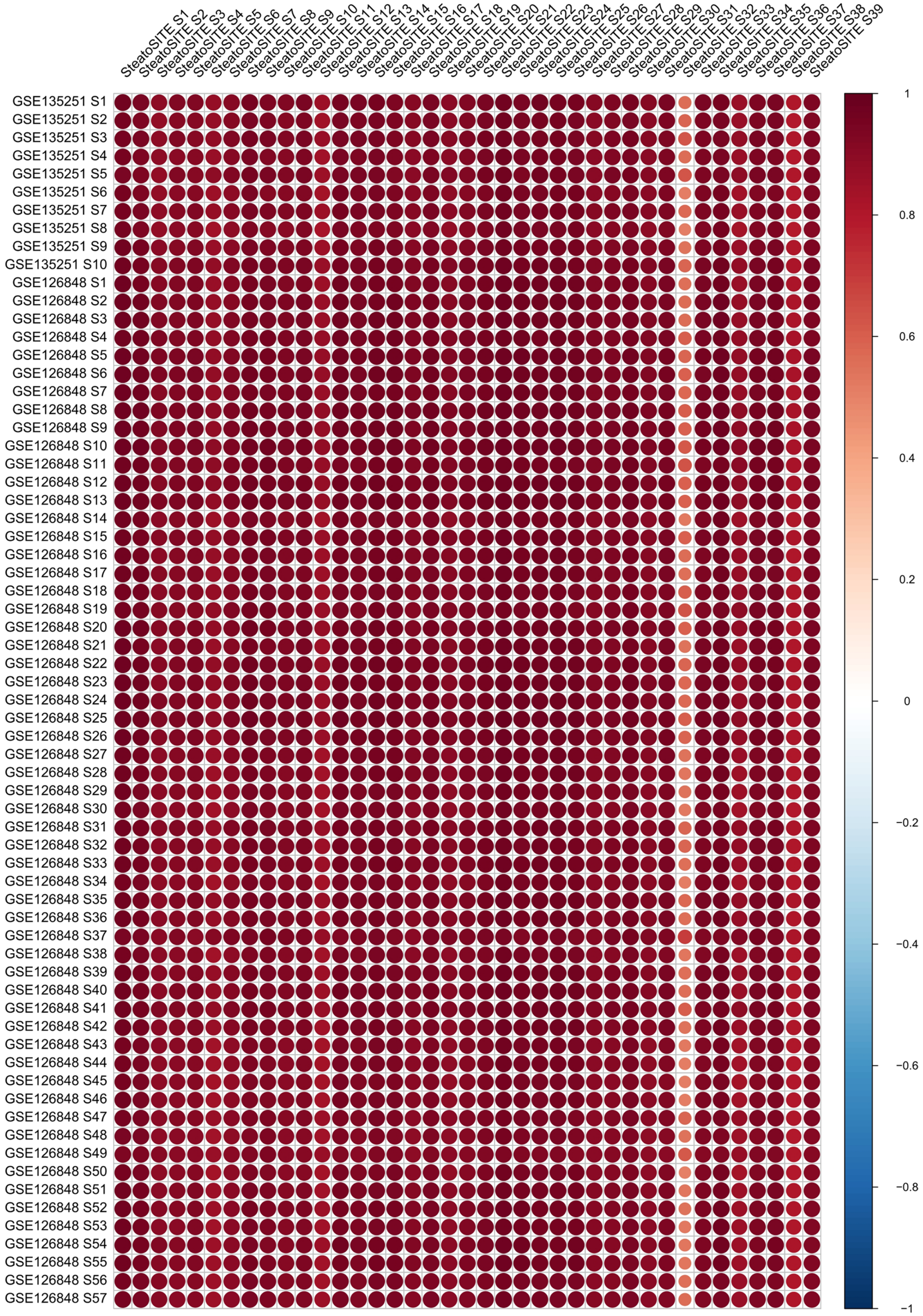

Extended Data Fig. 2 | Validation of normal liver transcriptome. Correlation (corrplot) of transcriptomic profiles of normal SteatoSITE samples (n = 39) with published normal liver reference data (n = 57). The colour scale corresponds to the strength and direction of correlations.

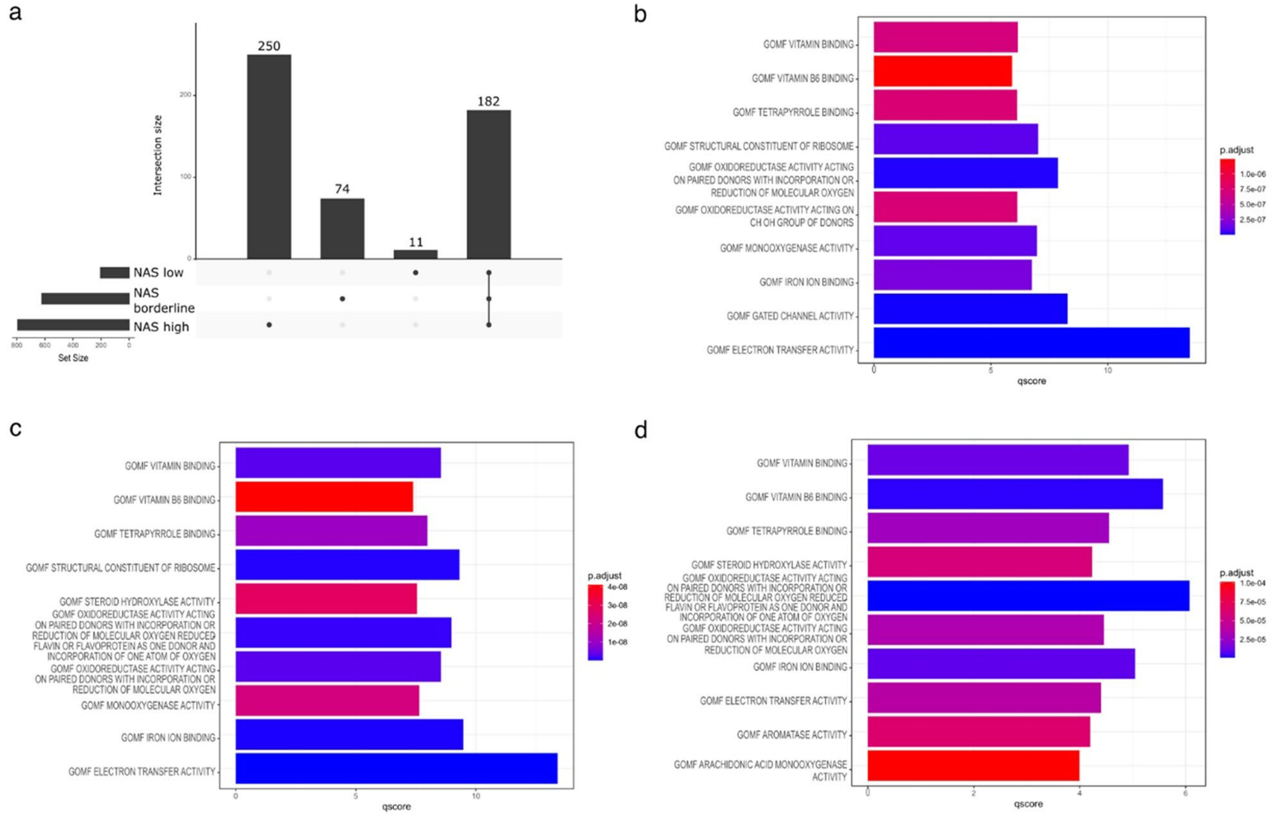

Extended Data Fig. 3 | SteatoSITE RNA-seq according to NAS scores. **a**, UpSet plot of differentially assessed genes (DEGs), showing DEGs belonging to individual sets (according to NAFLD activity score (NAS) ≤ 2, NAS 3/4 and NAS ≥ 5) and the intersection of DEGs across all NAS sets. Set sizes are presented as bars and their composition is described by the bottom panel. **b**, Top 10 molecular functions (gene ontology (GO) terms) identified with one-sided gene set enrichment analysis based on the differentially expressed genes of NAS ≤ 2; **c**, NAS 3/4; **d**, NAS ≥ 5 (Benjamin and Hochberg false discovery rate q < 0.05 and fold-change of ≥1).

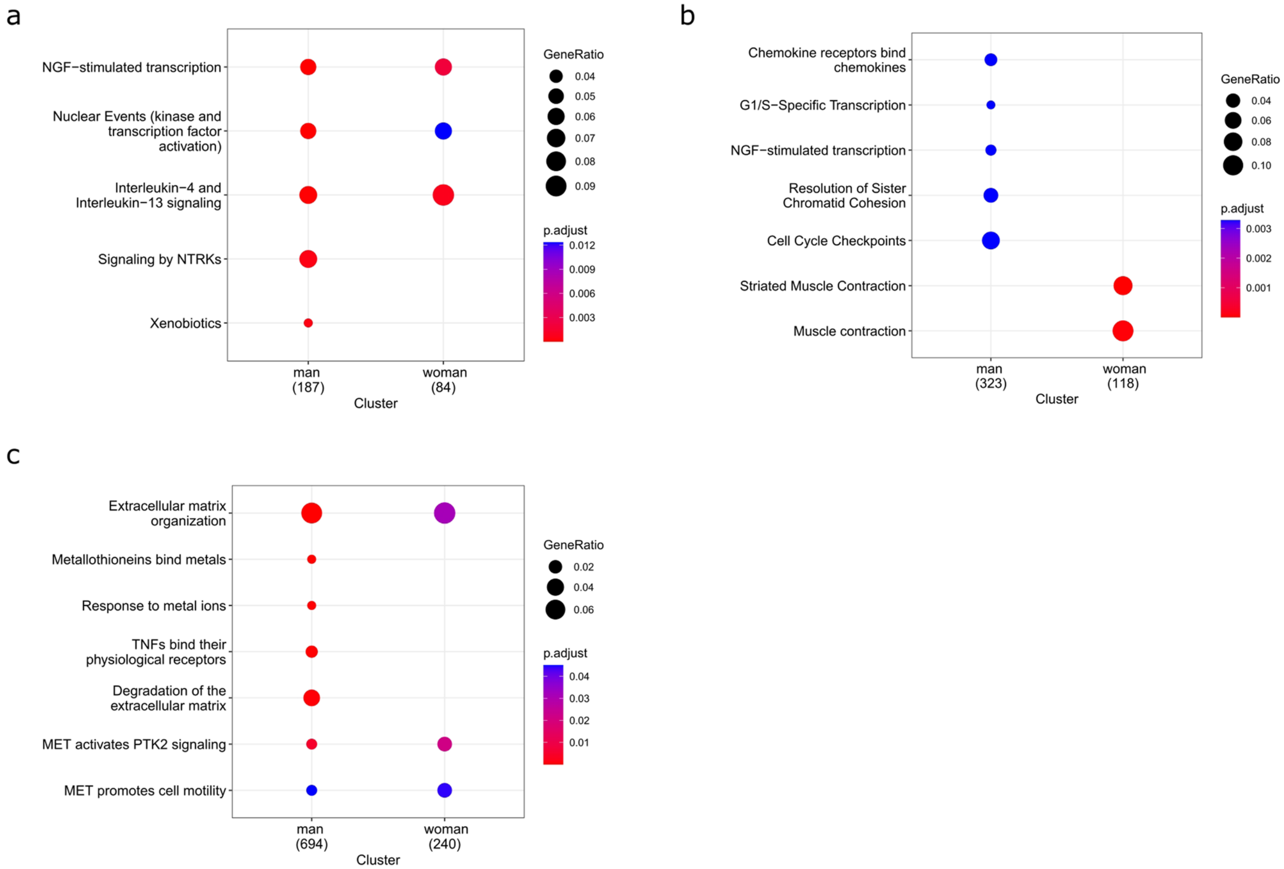

Extended Data Fig. 4 | SteatoSITE RNA-seq gender-focused gene enrichment analysis. Reactome pathways obtained from one-sided gene set enrichment analysis in both men and women for **a**, F0/1 vs control; **b**, F2 vs controls; **c**, F3 vs controls (Benjamin and Hochberg false discovery rate q < 0.05 and fold-change ≥ 1).

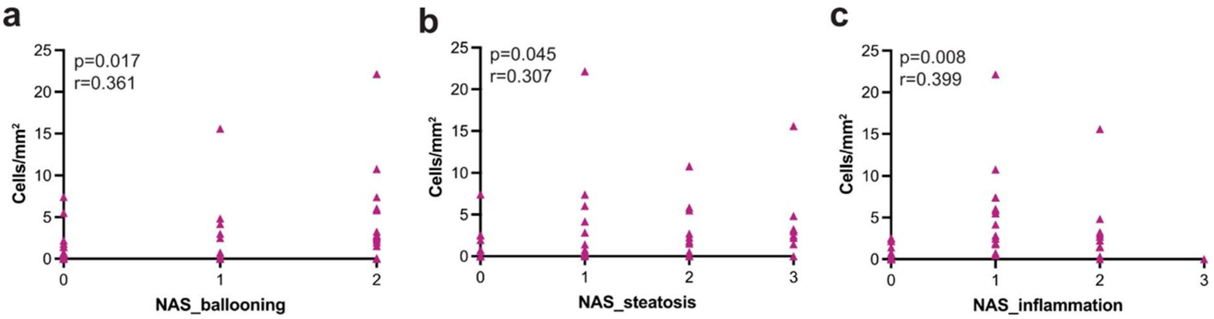

Extended Data Fig. 5 | Correlation of scar-associated macrophage numbers with NAFLD activity score components. Scar-associated macrophage numbers determined by multiplex immunofluorescence correlated positively with assigned components of the NAFLD activity score (n = 43). Spearman's rho and *P*-value indicated for ballooning (**a**), steatosis (**b**), and inflammation (**c**).

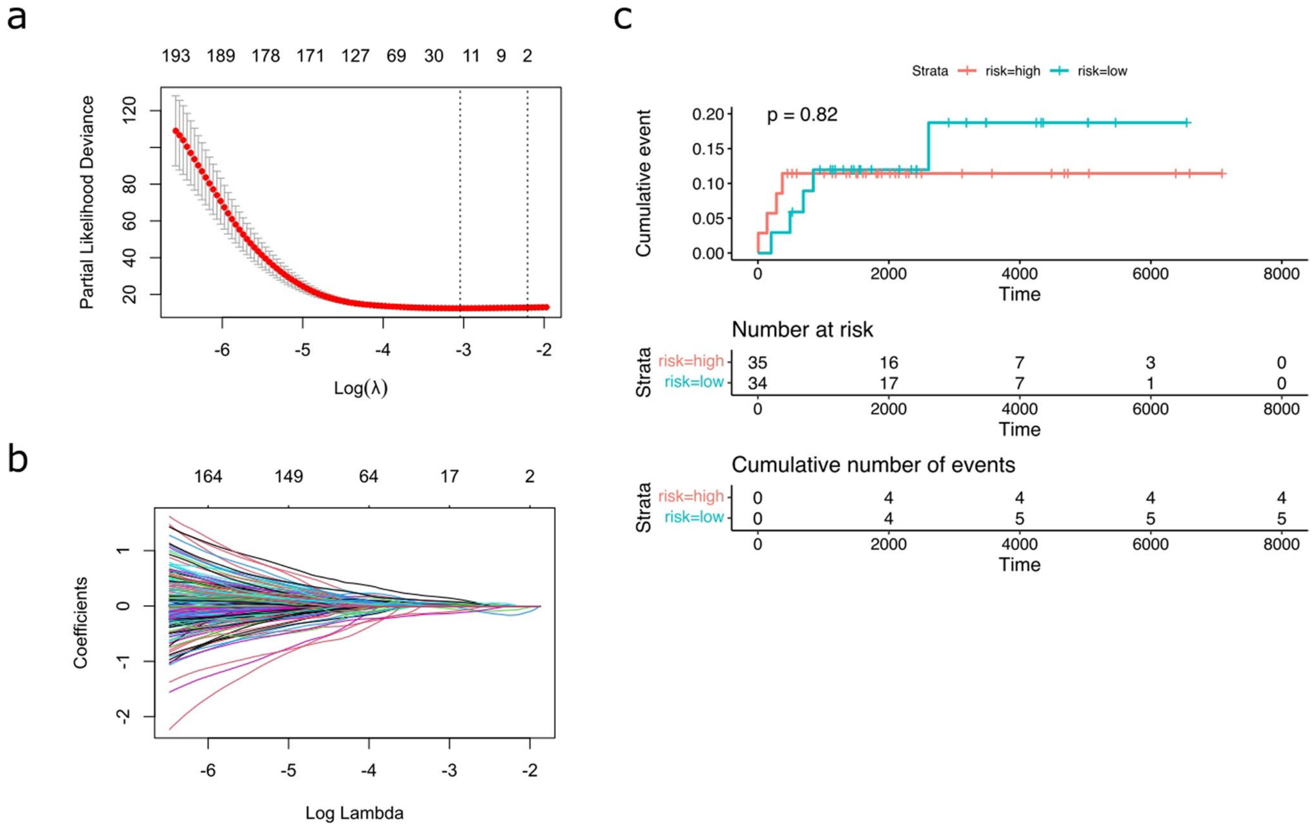

Extended Data Fig. 6 | Regularised Cox regression model. a, Plot of the optimal value of logarithmic lambda ($n = 100$) and the cross-validation error. Data presented as mean value +/− SD. **b**, Coefficient values across the logarithmic lambda. **c**, Kaplan-Meier plot demonstrating no separation of the event curves of patients with biopsies showing F2 fibrosis using the transcriptional risk score; log rank test P-value = 0.82.

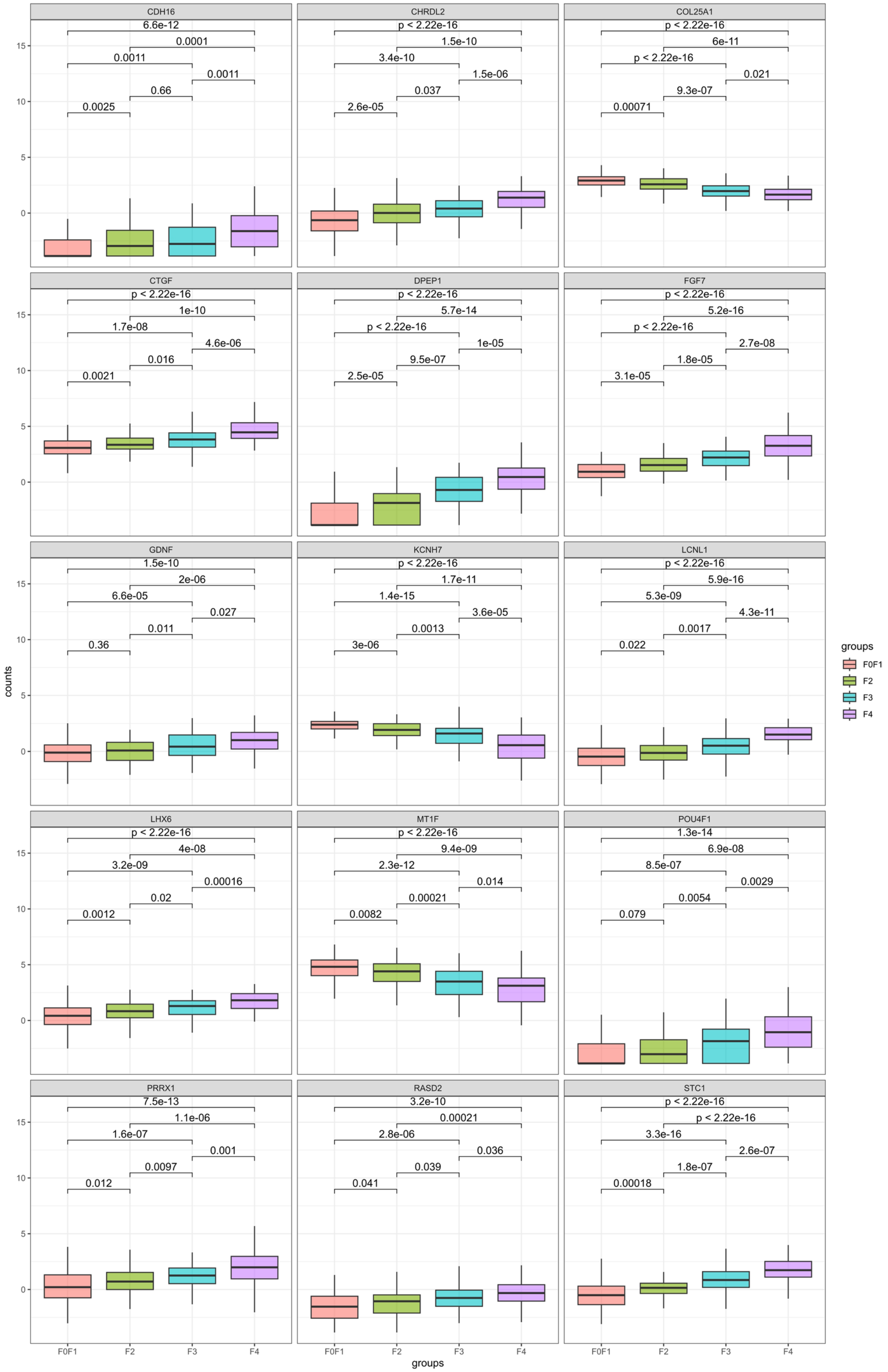

Extended Data Fig. 7 | Gene expression of the prognostic signature across the fibrotic stages. Plots of the normalised expression of the named 15 gene constituents of the transcriptional risk score by NASH-CRN fibrosis stage ($n = 368$), as visualised by the Shiny transcriptome browser app. All boxplots show median (centre line), first and third quartiles (lower and upper box limits), 1.5× interquartile range (whiskers). *P*-values of one-way ANOVA with post-hoc Tukey test.

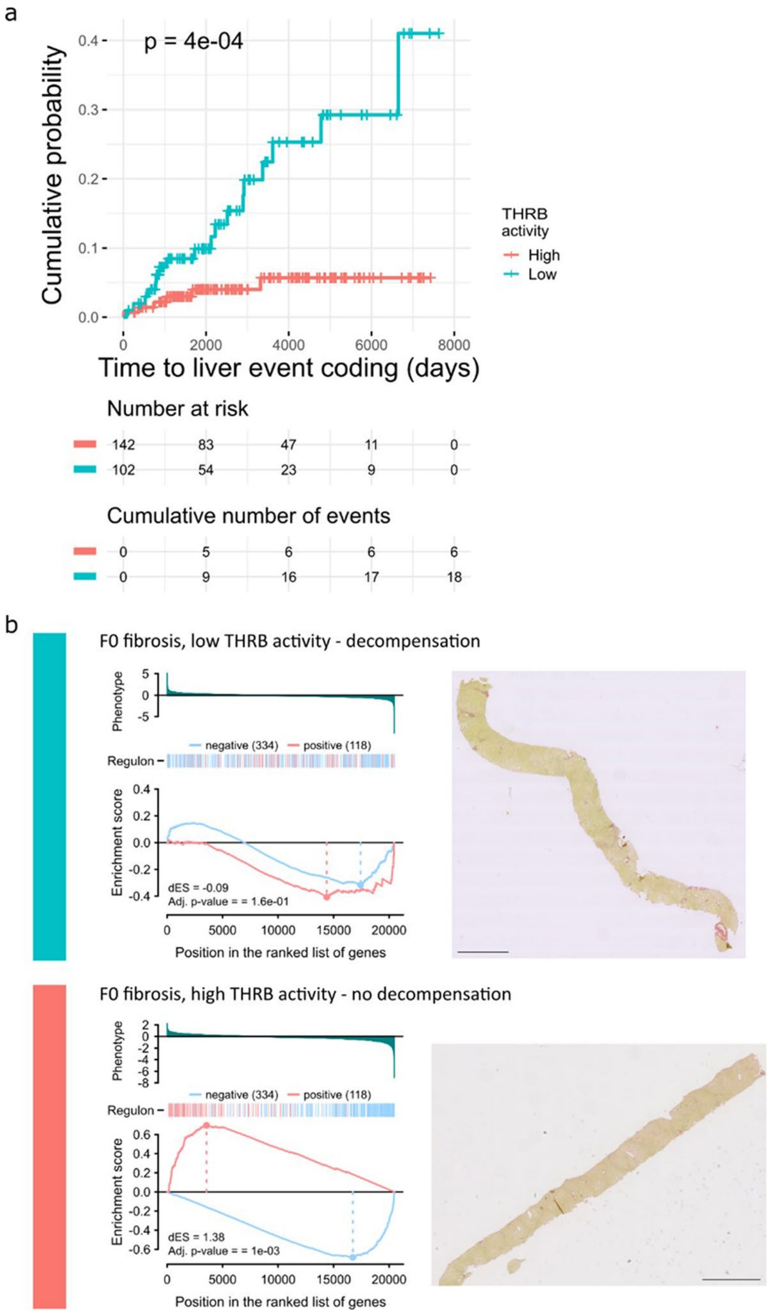

Extended Data Fig. 8 | Additional predictive and personalisation value of estimated THRB regulon activity in F0 and F1 stage disease. a, In histologically identical low-risk fibrosis stages (F0 and F1 biopsy cases), low THRB activity identifies patients at high risk of progression to a hepatic decompensation event; log rank test *P*-value. **b**, Example individual 2-tailed gene set enrichment plots of target genes in the THRB regulon (left, 2-tailed gene set enrichment testing with Benjamini and Hochberg (false discovery rate) adjusted *P*-values) from two patients with identical F0 stage (no scarring) on PSR stained sections (right), where the patient with low THRB differential regulon activity (top, blue) progressed to a hepatic decompensation event 3000 days after biopsy in contrast to a patient with high THRB regulon activity who did not experience a decompensation event during the 4400 days until censoring (bottom, red). Scale bars, 2 mm.

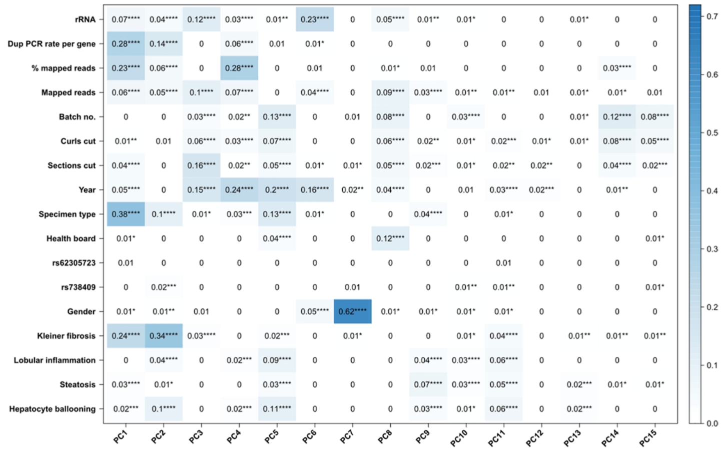

Extended Data Fig. 9 | Correlations between the main principal components and the clinical data. *P*-values of Spearman correlation test. * $P < 0.05$, ** $P < 0.01$, ** $P < 0.001$, **** $P < 0.0001$.

nature portfolio

Corresponding author(s): Professor Jonathan Fallowfield

Last updated by author(s): 19/09/23

Reporting Summary

Nature Portfolio wishes to improve the reproducibility of the work that we publish. This form provides structure for consistency and transparency in reporting. For further information on Nature Portfolio policies, see our Editorial Policies and the Editorial Policy Checklist.

Statistics

For all statistical analyses, confirm that the following items are present in the figure legend, table legend, main text, or Methods section.

n/a | Confirmed

□ ☒ The exact sample size (n) for each experimental group/condition, given as a discrete number and unit of measurement

□ ☒ A statement on whether measurements were taken from distinct samples or whether the same sample was measured repeatedly

□ ☒ The statistical test(s) used AND whether they are one- or two-sided
Only common tests should be described solely by name; describe more complex techniques in the Methods section.

□ ☒ A description of all covariates tested

□ ☒ A description of any assumptions or corrections, such as tests of normality and adjustment for multiple comparisons

□ ☒ A full description of the statistical parameters including central tendency (e.g. means) or other basic estimates (e.g. regression coefficient) AND variation (e.g. standard deviation) or associated estimates of uncertainty (e.g. confidence intervals)

□ ☒ For null hypothesis testing, the test statistic (e.g. F, t, r) with confidence intervals, effect sizes, degrees of freedom and P value noted
Give P values as exact values whenever suitable.

☒ □ For Bayesian analysis, information on the choice of priors and Markov chain Monte Carlo settings

☒ □ For hierarchical and complex designs, identification of the appropriate level for tests and full reporting of outcomes

□ ☒ Estimates of effect sizes (e.g. Cohen's d, Pearson's r), indicating how they were calculated

Our web collection on statistics for biologists contains articles on many of the points above.

Software and code

Policy information about availability of computer code

Data collection	A custom Python (version 3.9) script was developed to carry out Electronic Health Record data processing tasks.
Data analysis	When scoring the liver pathology, for ordinal variables, Light's kappa (square weighted, for >2 raters) was calculated using the 'psy' package (version 1.2), and intraclass correlation coefficient, Krippendorf's alpha, and Kendall's W were calculated using the 'irr' package (version 0.84.1) in R (version 4.1.0). Q Path open source software (version 0.2.3) was used for liver histopathological image analysis. Analysis using clinical and histopathological data only was undertaken in R (version 4.1.0) using the packages 'survival' (version 3.2-1), 'survminer' (version 0.4.9), and 'finalfit' (version 1.0.5). NeoGenomics used a proprietary deep learning-based workflow NeoLYTX (version 2.0) to identify individual liver cells and perform cell classification for cell markers. For RNA-seq analysis, the following software packages were used in R (version 4.1.2) : Reads were trimmed using 'Cutadapt' (version cutadapt-1.9.dev2) and aligned to the reference genome using 'STAR' (version 2.5.2b). Reads were assigned to features using 'featureCounts3' (version 1.5.1) with a igtf file from Ensembl (annotation version 84). Differential gene expression analysis was performed using limma-voom' (version 3.28.14); Gene Set Enrichment Analysis (GSEA) was performed with GSEA function from 'clusterProfiler' (version 4.0.5); data were visualized with 'ggplot2' (version 3.3.5) and 'clusterProfiler'; Cox regression was performed using 'glmnet' (version 4.1-4), and time-dependent ROC curves were created by the 'timeROC' package (version 0.4); Kaplan-Meier analysis was performed using 'survival' (version 3.4-0) and 'survminer' (version 0.4.9) packages. Genome Analysis Toolkit (GATK, version 4.0.1.2) was used to call genotypes. The MUlti-Subject Single Cell ('MuSiC') deconvolution tool (version 0.1.1) was run using R (version 3.6.3) for deconvolution analysis. The R package `ppcor' (version 1.1) was used to assess the correlation between the proportion of hepatic cell subtypes and the histological score or clinical outcomes.

Transcriptional network inference and regulon analysis was undertaken in R (version 4.1.0) using the 'RTN' package (version 2.16.0) implementing the ARACHNe algorithm, the 'RTNsurvival' package (version 1.16.0), 'maxstat' package (version 0.7-25), and 'Mfuzz' package (version 2.52.0).
An R Shiny app was used to develop the gene browser.
R scripts enabling the main steps of the analysis are available from the corresponding author on reasonable request.

For manuscripts utilizing custom algorithms or software that are central to the research but not yet described in published literature, software must be made available to editors and reviewers. We strongly encourage code deposition in a community repository (e.g. GitHub). See the Nature Portfolio guidelines for submitting code & software for further information.

Data

Policy information about availability of data

All manuscripts must include a data availability statement. This statement should provide the following information, where applicable:

- Accession codes, unique identifiers, or web links for publicly available datasets
- A description of any restrictions on data availability
- For clinical datasets or third party data, please ensure that the statement adheres to our policy

Hepatic bulk RNA-seq data is deposited in the European Nucleotide Archive (https://www.ebi.ac.uk/ena; study accession number: PRJEB58625). Gene expression data is also freely available for user-friendly interactive browsing online at https://shiny.igc.ed.ac.uk/SteatoSITE_gene_explorer/. SteatoSITE has delegated ethics from West of Scotland Research Ethics Committee 4 (Reference: 20/WS/0002; 18th February 2020) allowing the granting of access to the full dataset (histopathology scoring, hepatic bulk RNA-seq data, Electronic Health Record data) only within the PMS-IC secure environment to third parties by application (full details at https://steatosite.com/researchers/), overseen and reviewed by the SteatoSITE Scientific Advisory Board.

Research involving human participants, their data, or biological material

Policy information about studies with human participants or human data. See also policy information about sex, gender (identity/presentation), and sexual orientation and race, ethnicity and racism.

Reporting on sex and gender

'Gender' is reported as stated in the Electronic Health Record. Both men and women are included in the cohort. Gender was used as a covariate in analysis as there are sex-related differences in NAFLD prevalence and outcome.

Reporting on race, ethnicity, or other socially relevant groupings

Ethnicity and SIMD (Scottish Index of. Multiple Deprivation) data were collected from national administrative datasets and are reported as ethnicity and social deprivation influence NAFLD prevalence and outcome.

Population characteristics

Covariate relevant population characteristics include age (mean 55.1 years), gender (55.4% men, 44.6% women), ethnicity (White 64.5%, Asian 2.3%, unknown ethnicity 33.2%), SIMD (1 (6.9%), 2 (8%), 3 (7.8%), 4 (7.9%), 5 (8%), 6 (6.2%), 7 (5.3%), 8 (3.5%), 9 (4.4%), 10 (5.9%), unknown SIMD (36.3%)), diabetes status (32% type 2 diabetes), body mass index (median 31.3), liver fibrosis stage (F0 (n=247), F1 (n=208), F2 (n=152), F3 (n=169), F4 (n=164)), and genotypic (SNP) status (PNPLA3: GG (16.8%), GC (27.8%) and CC (54.7%).

Recruitment

This was a retrospective, observational study. Initial case selection was based on the availability of archival liver tissue (from biopsies, resections, or explants that were surplus to diagnosis) in formalin-fixed paraffin-embedded (FFPE) blocks available within the NHS Research Scotland Biorepository network, with the clinical and/or histological diagnosis of NAFLD, and meeting specific inclusion/exclusion criteria.
Using a secondary care tissue-first selection process introduces spectrum bias and this is acknowledged in the discussion. This is a strength in terms of outcome enrichment but means that SteatoSITE will have less value for modelling the population-level natural history of NAFLD.

Ethics oversight

Anonymised tissue was supplied after approval by the National Health Service Research Scotland (NRS) Biorepository network (Reference: SR1032; 2nd August 2018). Unified transparent approval for data inclusion in this pan-Scotland project was provided by the West of Scotland Research Ethics Committee 4 (Reference: 20/WS/0002; 18th February 2020), Public Benefit and Privacy Panel for Health and Social Care (PBPP; Reference: 1819-0091; 4th June 2021), Institutional Research & Development departments and Caldicott Guardians.

Note that full information on the approval of the study protocol must also be provided in the manuscript.

Field-specific reporting

Please select the one below that is the best fit for your research. If you are not sure, read the appropriate sections before making your selection.

☒ Life sciences □ Behavioural & social sciences □ Ecological, evolutionary & environmental sciences

For a reference copy of the document with all sections, see nature.com/documents/nr-reporting-summary-flat.pdf

Life sciences study design

All studies must disclose on these points even when the disclosure is negative.

Sample size

No sample size calculation was performed. The cohort size is a reflection of the maximum number of eligible cases across all of the Scottish

Sample size

Biorepositories at the time of data collection. To our knowledge, this is the largest collection of NAFLD cases with hepatic RNA-sequencing, digital pathology and linked clinical outcomes worldwide.

Data exclusions

There were pre-determined Quality Control criteria for RNA-sequencing (including RNA yield (and any potential DNA contamination) and DV200). Samples with DV200 below 30% were not progressed for sequencing but were included in other analyses (e.g., histopathological assessment).

Replication

We have established a unique resource to be used by the liver research community and to catalyze new discoveries in NAFLD. We present initial analyses to illustrate the utility of SteatoSITE. We used automated variable selection methods to reduce overfitting, but acknowledge that the 15-gene transcriptional risk score will require external validation if suitable cohorts can be identified

Randomization

There were no randomization procedures employed - this was a retrospective observational study. For RNA-seq analysis, principal component analysis (PCA) was performed to identify covariates that significantly correlated with the main principal components, so they could be controlled for downstream analyses. For this reason, sex was included as an additive effect in the linear model used for differential expression

Blinding

All cases were assigned a unique study ID (and the key only held by the NRS Biorepositories). Histopathological assessors and RNA-sequencing analysts were blinded to any patient information. Bioinformaticians only accessed the clinical outcome data after histopathological scoring and RNAseq analysis had been performed to enable time-to-event analysis/risk prediction etc.

Behavioural & social sciences study design

All studies must disclose on these points even when the disclosure is negative.

Study description

Briefly describe the study type including whether data are quantitative, qualitative, or mixed-methods (e.g. qualitative cross-sectional, quantitative experimental, mixed-methods case study).

Research sample

State the research sample (e.g. Harvard university undergraduates, villagers in rural India) and provide relevant demographic information (e.g. age, sex) and indicate whether the sample is representative. Provide a rationale for the study sample chosen. For studies involving existing datasets, please describe the dataset and source.

Sampling strategy

Describe the sampling procedure (e.g. random, snowball, stratified, convenience). Describe the statistical methods that were used to predetermine sample size OR if no sample-size calculation was performed, describe how sample sizes were chosen and provide a rationale for why these sample sizes are sufficient. For qualitative data, please indicate whether data saturation was considered, and what criteria were used to decide that no further sampling was needed.

Data collection

Provide details about the data collection procedure, including the instruments or devices used to record the data (e.g. pen and paper, computer, eye tracker, video or audio equipment) whether anyone was present besides the participant(s) and the researcher, and whether the researcher was blind to experimental condition and/or the study hypothesis during data collection.

Timing

Indicate the start and stop dates of data collection. If there is a gap between collection periods, state the dates for each sample cohort.

Data exclusions

If no data were excluded from the analyses, state so OR if data were excluded, provide the exact number of exclusions and the rationale behind them, indicating whether exclusion criteria were pre-established.

Non-participation

State how many participants dropped out/declined participation and the reason(s) given OR provide response rate OR state that no participants dropped out/declined participation.

Randomization

If participants were not allocated into experimental groups, state so OR describe how participants were allocated to groups, and if allocation was not random, describe how covariates were controlled.

Ecological, evolutionary & environmental sciences study design

All studies must disclose on these points even when the disclosure is negative.

Study description

Briefly describe the study. For quantitative data include treatment factors and interactions, design structure (e.g. factorial, nested, hierarchical), nature and number of experimental units and replicates.

Research sample

Describe the research sample (e.g. a group of tagged Passer domesticus, all Stenocereus thurberi within Organ Pipe Cactus National Monument), and provide a rationale for the sample choice. When relevant, describe the organism taxa, source, sex, age range and any manipulations. State what population the sample is meant to represent when applicable. For studies involving existing datasets, describe the data and its source.

Sampling strategy

Note the sampling procedure. Describe the statistical methods that were used to predetermine sample size OR if no sample-size calculation was performed, describe how sample sizes were chosen and provide a rationale for why these sample sizes are sufficient.

Data collection

Describe the data collection procedure, including who recorded the data and how.

Timing and spatial scale

Indicate the start and stop dates of data collection, noting the frequency and periodicity of sampling and providing a rationale for

Timing and spatial scale	*these choices. If there is a gap between collection periods, state the dates for each sample cohort. Specify the spatial scale from which the data are taken*
Data exclusions	*If no data were excluded from the analyses, state so OR if data were excluded, describe the exclusions and the rationale behind them, indicating whether exclusion criteria were pre-established.*
Reproducibility	*Describe the measures taken to verify the reproducibility of experimental findings. For each experiment, note whether any attempts to repeat the experiment failed OR state that all attempts to repeat the experiment were successful.*
Randomization	*Describe how samples/organisms/participants were allocated into groups. If allocation was not random, describe how covariates were controlled. If this is not relevant to your study, explain why.*
Blinding	*Describe the extent of blinding used during data acquisition and analysis. If blinding was not possible, describe why OR explain why blinding was not relevant to your study.*

Did the study involve field work? □ Yes □ No

Field work, collection and transport

Field conditions	*Describe the study conditions for field work, providing relevant parameters (e.g. temperature, rainfall).*
Location	*State the location of the sampling or experiment, providing relevant parameters (e.g. latitude and longitude, elevation, water depth).*
Access & import/export	*Describe the efforts you have made to access habitats and to collect and import/export your samples in a responsible manner and in compliance with local, national and international laws, noting any permits that were obtained (give the name of the issuing authority, the date of issue, and any identifying information).*
Disturbance	*Describe any disturbance caused by the study and how it was minimized.*

Reporting for specific materials, systems and methods

We require information from authors about some types of materials, experimental systems and methods used in many studies. Here, indicate whether each material, system or method listed is relevant to your study. If you are not sure if a list item applies to your research, read the appropriate section before selecting a response.

Materials & experimental systems

n/a	Involved in the study	
□	☒	Antibodies
□	□	Eukaryotic cell lines
□	□	Palaeontology and archaeology
□	□	Animals and other organisms
□	☒	Clinical data
□	□	Dual use research of concern
□	□	Plants

Methods

n/a	Involved in the study	
□	□	ChIP-seq
□	□	Flow cytometry
□	□	MRI-based neuroimaging

Antibodies

Antibodies used	Antibodies for MultiOmyx analysis: by staining order, were rabbit anti-TREM2 (polyclonal, ProteinTech, Catalog# 13483-1-AP, Vendor Lot ID NG) mouse anti-MNDA (253A, Abcam, Catalog# ab270556, Vendor Lot ID GR3326911), rabbit anti-CD9 (EPR2949, Abcam, Catalog# ab195422, Vendor Lot ID GR3282696), mouse anti-CD66b (G10F5, BioLegend, Catalog# 93231, ,Vendor Lot ID B276347), mouse anti-CD11B (238439, R&D Systems, Catalog# MAB16992, Vendor Lot ID KGZ0418101), rabbit anti-DC-SIGN (D7F5C, Cell Signaling Technology, Catalog# 13193, Vendor Lot ID 2), rabbit anti-Ki67 (SP6, Abcam Catalog# ab231172, Vendor Lot ID GR3277378), rabbit anti-IDO1 (SP260, Abcam Catalog# ab228468, Vendor Lot ID GR3208566), rabbit anti¬CD11c (D3V1E, Cell Signaling Catalog# 45581BF, Vendor Lot ID 2), rabbit anti-PD-L1 (SP142, Abcam Catalog# ab236238, Vendor Lot ID GR3246745), rabbit anti-CD14 (EPR3652, Abcam Catalog# ab209971, Vendor Lot ID GR316076), mouse anti-CD16 (DJ130c, ThermoFisher Scientific Catalog# MA1-84008, Vendor Lot ID TK2673378), mouse anti-CD68 (KP1, BioLegend Catalog# 98998, Vendor Lot ID B297229), mouse anti-CD163 (EDHu-1, Bio-Rad Catalog# MCA1853, Vendor Lot ID 149022A), mouse anti-HLA DQ/DR/DP (WR18, Novus Catalog# NB100-64358, Vendor Lot ID 1808), mouse anti-CD33 (44M12D3, Novus Biologicals Catalog# NBP2-22377, Vendor Lot ID 1127455612D3), mouse anti-SMA (1A4, Sigma-Aldrich Catalog# A5228, Vendor Lot ID 037M4805V).
Validation	The specificity of all antibodies was validated by board-certified pathologists employed by NeoGenomics.

Eukaryotic cell lines

Policy information about cell lines and Sex and Gender in Research

Cell line source(s)

State the source of each cell line used and the sex of all primary cell lines and cells derived from human participants or vertebrate models.

Authentication

Describe the authentication procedures for each cell line used OR declare that none of the cell lines used were authenticated.

Mycoplasma contamination

Confirm that all cell lines tested negative for mycoplasma contamination OR describe the results of the testing for mycoplasma contamination OR declare that the cell lines were not tested for mycoplasma contamination.

Commonly misidentified lines
(See ICLAC register)

Name any commonly misidentified cell lines used in the study and provide a rationale for their use.

Palaeontology and Archaeology

Specimen provenance

Provide provenance information for specimens and describe permits that were obtained for the work (including the name of the issuing authority, the date of issue, and any identifying information). Permits should encompass collection and, where applicable, export.

Specimen deposition

Indicate where the specimens have been deposited to permit free access by other researchers.

Dating methods

If new dates are provided, describe how they were obtained (e.g. collection, storage, sample pretreatment and measurement), where they were obtained (i.e. lab name), the calibration program and the protocol for quality assurance OR state that no new dates are provided.

□ Tick this box to confirm that the raw and calibrated dates are available in the paper or in Supplementary Information.

Ethics oversight

Identify the organization(s) that approved or provided guidance on the study protocol, OR state that no ethical approval or guidance was required and explain why not.

Note that full information on the approval of the study protocol must also be provided in the manuscript.

Animals and other research organisms

Policy information about studies involving animals; ARRIVE guidelines recommended for reporting animal research, and Sex and Gender in Research

Laboratory animals

For laboratory animals, report species, strain and age OR state that the study did not involve laboratory animals.

Wild animals

Provide details on animals observed in or captured in the field; report species and age where possible. Describe how animals were caught and transported and what happened to captive animals after the study (if killed, explain why and describe method; if released, say where and when) OR state that the study did not involve wild animals.

Reporting on sex

Indicate if findings apply to only one sex; describe whether sex was considered in study design, methods used for assigning sex. Provide data disaggregated for sex where this information has been collected in the source data as appropriate; provide overall numbers in this Reporting Summary. Please state if this information has not been collected. Report sex-based analyses where performed, justify reasons for lack of sex-based analysis.

Field-collected samples

For laboratory work with field-collected samples, describe all relevant parameters such as housing, maintenance, temperature, photoperiod and end-of-experiment protocol OR state that the study did not involve samples collected from the field.

Ethics oversight

Identify the organization(s) that approved or provided guidance on the study protocol, OR state that no ethical approval or guidance was required and explain why not.

Note that full information on the approval of the study protocol must also be provided in the manuscript.

Clinical data

Policy information about clinical studies

All manuscripts should comply with the ICMJE guidelines for publication of clinical research and a completed CONSORT checklist must be included with all submissions.

Clinical trial registration

This was not a clinical trial.

Study protocol

This was not a clinical trial. Full methodological details are provided in the manuscript.

Data collection

A total of 940 cases from the three participating NHS Scotland Biorepositories (Lothian, Greater Glasgow & Clyde, and Grampian) were included, representing the full histological spectrum from normal liver tissue to NAFLD-related cirrhosis. Cases with a liver tissue sample acquired between January 2000 and October 2019 were selected. All patients were years of age at the tissue sampling date. Data from Electronic Health Records and national datasets were retrieved, where available, from a period between ten years before the tissue sampling date until May 2020.

Outcomes

We collected all relevant clinical outcomes according to recent expert consensus guidelines for using administrative coding in Electronic Health Record-based research of NAFLD.

Dual use research of concern

Policy information about dual use research of concern

Hazards

Could the accidental, deliberate or reckless misuse of agents or technologies generated in the work, or the application of information presented in the manuscript, pose a threat to:

No | Yes

☒ ☐ Public health

☒ ☐ National security

☒ ☐ Crops and/or livestock

☒ ☐ Ecosystems

☒ ☐ Any other significant area

Experiments of concern

Does the work involve any of these experiments of concern:

No | Yes

☒ ☐ Demonstrate how to render a vaccine ineffective

☒ ☐ Confer resistance to therapeutically useful antibiotics or antiviral agents

☒ ☐ Enhance the virulence of a pathogen or render a nonpathogen virulent

☒ ☐ Increase transmissibility of a pathogen

☒ ☐ Alter the host range of a pathogen

☒ ☐ Enable evasion of diagnostic/detection modalities

☒ ☐ Enable the weaponization of a biological agent or toxin

☒ ☐ Any other potentially harmful combination of experiments and agents

Plants

Seed stocks

Report on the source of all seed stocks or other plant material used. If applicable, state the seed stock centre and catalogue number. If plant specimens were collected from the field, describe the collection location, date and sampling procedures.

Novel plant genotypes

Describe the methods by which all novel plant genotypes were produced. This includes those generated by transgenic approaches, gene editing, chemical/radiation-based mutagenesis and hybridization. For transgenic lines, describe the transformation method, the number of independent lines analyzed and the generation upon which experiments were performed. For gene-edited lines, describe the editor used, the endogenous sequence targeted for editing, the targeting guide RNA sequence (if applicable) and how the editor was applied.

Authentication

Describe any authentication procedures for each seed stock used or novel genotype generated. Describe any experiments used to assess the effect of a mutation and, where applicable, how potential secondary effects (e.g. second site T-DNA insertions, mosiacism, off-target gene editing) were examined.

ChIP-seq

Data deposition

☐ Confirm that both raw and final processed data have been deposited in a public database such as GEO.

☐ Confirm that you have deposited or provided access to graph files (e.g. BED files) for the called peaks.

Data access links
May remain private before publication.

For "Initial submission" or "Revised version" documents, provide reviewer access links. For your "Final submission" document, provide a link to the deposited data.

Files in database submission

Provide a list of all files available in the database submission.

Genome browser session (e.g. UCSC)	*Provide a link to an anonymized genome browser session for "Initial submission" and "Revised version" documents only, to enable peer review. Write "no longer applicable" for "Final submission" documents.*

Methodology

Replicates	*Describe the experimental replicates, specifying number, type and replicate agreement.*
Sequencing depth	*Describe the sequencing depth for each experiment, providing the total number of reads, uniquely mapped reads, length of reads and whether they were paired- or single-end.*
Antibodies	*Describe the antibodies used for the ChIP-seq experiments; as applicable, provide supplier name, catalog number, clone name, and lot number.*
Peak calling parameters	*Specify the command line program and parameters used for read mapping and peak calling, including the ChIP, control and index files used.*
Data quality	*Describe the methods used to ensure data quality in full detail, including how many peaks are at FDR 5% and above 5-fold enrichment.*
Software	*Describe the software used to collect and analyze the ChIP-seq data. For custom code that has been deposited into a community repository, provide accession details.*

Flow Cytometry

Plots

Confirm that:

□ The axis labels state the marker and fluorochrome used (e.g. CD4-FITC).

□ The axis scales are clearly visible. Include numbers along axes only for bottom left plot of group (a 'group' is an analysis of identical markers).

□ All plots are contour plots with outliers or pseudocolor plots.

□ A numerical value for number of cells or percentage (with statistics) is provided.

Methodology

Sample preparation	*Describe the sample preparation, detailing the biological source of the cells and any tissue processing steps used.*
Instrument	*Identify the instrument used for data collection, specifying make and model number.*
Software	*Describe the software used to collect and analyze the flow cytometry data. For custom code that has been deposited into a community repository, provide accession details.*
Cell population abundance	*Describe the abundance of the relevant cell populations within post-sort fractions, providing details on the purity of the samples and how it was determined.*
Gating strategy	*Describe the gating strategy used for all relevant experiments, specifying the preliminary FSC/SSC gates of the starting cell population, indicating where boundaries between "positive" and "negative" staining cell populations are defined.*

□ Tick this box to confirm that a figure exemplifying the gating strategy is provided in the Supplementary Information.

Magnetic resonance imaging

Experimental design

Design type	*Indicate task or resting state; event-related or block design.*
Design specifications	*Specify the number of blocks, trials or experimental units per session and/or subject, and specify the length of each trial or block (if trials are blocked) and interval between trials.*
Behavioral performance measures	*State number and/or type of variables recorded (e.g. correct button press, response time) and what statistics were used to establish that the subjects were performing the task as expected (e.g. mean, range, and/or standard deviation across subjects).*

Acquisition

Imaging type(s) *Specify: functional, structural, diffusion, perfusion.*

Field strength *Specify in Tesla*

Sequence & imaging parameters *Specify the pulse sequence type (gradient echo, spin echo, etc.), imaging type (EPI, spiral, etc.), field of view, matrix size, slice thickness, orientation and TE/TR/flip angle.*

Area of acquisition *State whether a whole brain scan was used OR define the area of acquisition, describing how the region was determined.*

Diffusion MRI □ Used □ Not used

Preprocessing

Preprocessing software *Provide detail on software version and revision number and on specific parameters (model/functions, brain extraction, segmentation, smoothing kernel size, etc.).*

Normalization *If data were normalized/standardized, describe the approach(es): specify linear or non-linear and define image types used for transformation OR indicate that data were not normalized and explain rationale for lack of normalization.*

Normalization template *Describe the template used for normalization/transformation, specifying subject space or group standardized space (e.g. original Talairach, MNI305, ICBM152) OR indicate that the data were not normalized.*

Noise and artifact removal *Describe your procedure(s) for artifact and structured noise removal, specifying motion parameters, tissue signals and physiological signals (heart rate, respiration).*

Volume censoring *Define your software and/or method and criteria for volume censoring, and state the extent of such censoring.*

Statistical modeling & inference

Model type and settings *Specify type (mass univariate, multivariate, RSA, predictive, etc.) and describe essential details of the model at the first and second levels (e.g. fixed, random or mixed effects; drift or auto-correlation).*

Effect(s) tested *Define precise effect in terms of the task or stimulus conditions instead of psychological concepts and indicate whether ANOVA or factorial designs were used.*

Specify type of analysis: □ Whole brain □ ROI-based □ Both

Statistic type for inference *Specify voxel-wise or cluster-wise and report all relevant parameters for cluster-wise methods.*

(See Eklund et al. 2016)

Correction *Describe the type of correction and how it is obtained for multiple comparisons (e.g. FWE, FDR, permutation or Monte Carlo).*

Models & analysis

n/a	Involved in the study
□	□ Functional and/or effective connectivity
□	□ Graph analysis
□	□ Multivariate modeling or predictive analysis

Functional and/or effective connectivity *Report the measures of dependence used and the model details (e.g. Pearson correlation, partial correlation, mutual information).*

Graph analysis *Report the dependent variable and connectivity measure, specifying weighted graph or binarized graph, subject- or group-level, and the global and/or node summaries used (e.g. clustering coefficient, efficiency, etc.).*

Multivariate modeling and predictive analysis *Specify independent variables, features extraction and dimension reduction, model, training and evaluation metrics.*